

Article

Atlas of Micromorphological Degradation of Archaeological Birch Bark

Johanna Klügl^{1,2,*}  and Giovanna Di Pietro²¹ Archaeological Service of the Canton Bern, Brünnenstrasse 66, 3018 Bern, Switzerland² Bern Academy of the Arts, Institute Materiality in Art and Culture, Fellerstrasse 11, 3027 Bern, Switzerland; giovanna.dipietro@bfh.ch

* Correspondence: johanna.kluegl@be.ch

Abstract: In this paper we present an atlas of micromorphological degradation of archaeological birch bark for the first time. We analysed the morphology of 13 samples extracted from ice-logged, waterlogged and cave-retrieved objects dated from the Neolithic to the Middle Age by means of light microscopy (LM) and transmission electron microscopy (TEM). We then compared their morphology to that of a contemporary sample, both intact and decayed. In all samples, 13 morphological characteristics that can be associated with fungal, bacterial, chemical, mechanical and light degradation are defined and described, and example LM and TEM images are provided. This novel atlas provides conservator-restorers a much-needed tool to relate the macroscopic appearance to the microscopic structure of birch bark objects. The most important macroscopic features allowing estimation of the state of preservation at the cell level are colour changes, loss of pliability, presence of delamination and increased brittleness. Colour change and delamination can be connected to microscopic features, and microscopic analysis can trace whether they were caused by biotic, chemical or physical decay. However, increased brittleness cannot be connected to a specific microscopic feature.



Citation: Klügl, J.; Di Pietro, G. Atlas of Micromorphological Degradation of Archaeological Birch Bark. *Appl. Sci.* **2021**, *11*, 8721. <https://doi.org/10.3390/app11188721>

Academic Editor: Maria Filomena Macedo

Received: 5 August 2021
Accepted: 14 September 2021
Published: 18 September 2021

Publisher's Note: MDPI stays neutral with regard to jurisdictional claims in published maps and institutional affiliations.



Copyright: © 2021 by the authors. Licensee MDPI, Basel, Switzerland. This article is an open access article distributed under the terms and conditions of the Creative Commons Attribution (CC BY) license (<https://creativecommons.org/licenses/by/4.0/>).

Keywords: phellem; birch bark; decay; fungi; bacteria; light microscopy; transmission electron microscopy; archaeology; ice patch; waterlogged

1. Introduction

Birch bark is a waterproof material that has been widely used since Mesolithic times because it is widely available and easily harvested and processed. In recent decades, some key archaeological objects made of birch bark have been discovered, among them a bow case from the Schnidejoch pass in the Swiss alps. Conservation strategies for birch bark objects often mimic those for wooden objects, but data on birch bark decay pathways are needed if appropriate conservation methods are to be developed. It is a well-known fact that archaeological wood suffers mainly from biodeterioration. When it dries in an uncontrolled way, the biotic decay of the cell walls results in cell shrinkage and collapse, macroscopically visible as severe volume reduction, warping, cracking and even disintegration. In order to develop appropriate drying procedures, it is therefore relevant to ask if birch bark suffers from similar biotic decay. To answer this question, we first review the current knowledge on the morphology, chemical composition and degradation of birch bark. Then, we present novel light microscopy and electron transmission microscopy results describing the macroscopic appearance and micromorphology of ice-logged, waterlogged and cave-retrieved samples dated from the Neolithic to the Middle Age and compare them with the morphology of intact, oxygen-exposed, decayed-in-nature contemporary samples.

Although degradation is always object-dependent, our aim is to present an atlas of possible micromorphological degradation patterns of archaeological objects made of birch bark in order to help conservator-restorers relate the macroscopic condition to the microscopic structure. This is a novel and much-needed tool that will help in assessing the

state of conservation of birch bark objects, the first step in making a decision about active and passive conservation measures.

1.1. Morphology of Birch Bark

The portion of the bark of the birch tree that is used to manufacture objects is the outer smooth white layer, called the phellem in botany. The function of the birch phellem is to prevent transpiration and to provide thermal [1] and parasite [2] protection. It consists of two cell types produced by the phellogen, arranged in alternating and compact radial layers, providing the characteristic laminated structure of the bark. One cell type has thin walls and a broad lumen filled with a white substance, betulin, while the second cell type has thick walls and a small lumen filled with a red-brown material composed of phenolic compounds [3–5] (Figure 1). The ratio of thin- to thick-walled cell layers depends on the *Betula* species and the specific tree history [3].

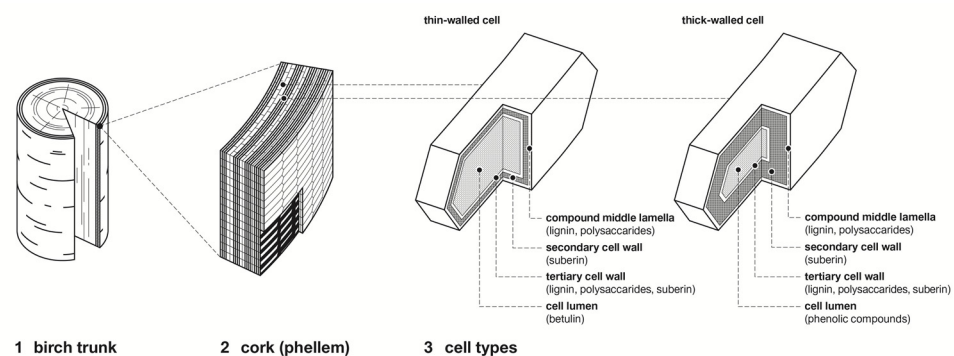


Figure 1. Schematic representation of the morphology and chemical composition of birch bark cells: 1. location of bark in trunk; 2. alternating layers of thick-walled and thin-walled phellem cells; 3. structure and chemical composition of thin- and thick-walled cells.

The cell walls are composed of a primary, secondary and tertiary layer, and the individual cells are joined together by the middle lamella, often called the compound middle lamella, as it can hardly be distinguished from the primary wall [6]. The phellem cells are arranged in such a way that the radial middle lamella creates a line. The thin-walled cells are heavily compressed in the outer portion of the bark but start off with a square shape. The compression and folding of the thin-walled cells can be explained by the formation of the phellem. To adjust to the growing size of the phellem, the bark cells are pushed outwards: the cells stretch in a tangential direction, while the thin-walled cells are compressed [7]. The folding of radial cell walls has also been observed in phellem of other trees, e.g., *Quercus suber* [8], *Pseudotsuga menziesii* [9] and *Prunus serrula* [10].

The secondary walls of both types of cells are composed of suberin, a biopolymer that makes the cork impermeable. Gas and water exchanges occur through characteristic openings called lenticels [11,12]. These are formed by fanned-out bands of continuous, heavily suberized, thick-walled cell layers and interrupted by void spaces filled with irregular cells. The intercellular spaces between the thick-walled cells visible in the lenticels' radial sections are absent in the normal phellem [12,13].

The suberization of the cell walls takes place after their generation from the phellogen [14]. In this phase, the channels connecting the cells, so-called plasmodesmata, become closed and the phellem cells die. Plasmodesmata with a diameter of 50 nm have been found mainly in tangential suberized cell walls of *Betula* sp. phellem [12]. Dead cells are less nutritious and have better resistance to microbial decay [15].

1.2. Chemical Composition of Birch Bark

The chemical composition of the outer bark of *Betula* sp. has been investigated several times [16–18]. The most recent analyses [19] confirm that it is composed of suberin (36.2%), lignin (14.3%) and polysaccharides (10.3%) located in the cell walls, and extractives

(32.2%) located in the cell lumen, specifically betulin in the thin-walled cells and phenolic compounds in the thick-walled cells [20]. Kiyoto and Sugiyama [21] recently elucidated the chemical composition of the different layers of the cell wall. The middle lamella and the primary cell wall are composed of lignin, cellulose and polysaccharides, the secondary cell wall by suberin, and the tertiary cell wall is subdivided into a middle layer with the same composition as the primary cell wall and a suberized inner layer (Figure 1). This composition was found in both cell types, and thin-walled cells have been reported to be less suberized than thick-walled cells [12]. Electron micrographs of suberized cell walls reveal a lamellar structure arising from the polyaliphatic and polyphenolic parts of suberin connected by glycerol via ester bonds. The light areas consist of aliphatic suberin, and the dark lamellae are rich in polyphenolic substances [22].

1.3. Degradation and Preservation Condition of Archaeological Birch Bark

Degradation of archaeological birch bark artefacts causes macroscopic colour fading [23], discoloration [24], delamination [25,26], deformation–distortion [27] and increased water absorption [28], but the connection between the burial conditions of archaeological bark and the dominant degradation pathways has never been investigated in detail. Different authors have shown that when Mesolithic and Neolithic archaeological birch bark artefacts are recovered from wetlands [29], caves [30,31] or waterlogged environments [32], they can be brittle and lose substance. This increased brittleness can have chemical and/or biological origins. Concerning the chemical origins, gas chromatography/mass spectrometry (GC/MS) examinations of waterlogged Neolithic alpine artefacts [25] detected depolymerization and oxidation, attributed to higher hydrolysis of susceptible groups, such as epoxy linkages.

Concerning the biological origins, investigations of artefacts recovered from the wetland site Star Carr dating from the ninth millennium BC revealed fungal hyphae within the bark structure, and pyrite and gypsum crystals on the surface [29]. The fragility of the artefacts was attributed to both the mineral deposits and the microbial attack. Gypsum crystals within the bark structure were also found in birch bark torches from the Kosacken-berg caves dated 2300–1800 BC and Iron Age [30], in a quiver from Xinjiang (Northwest China) dated 618–907 AD [33] and in Bronze Age barks from salt mines [34]. Specific investigations of the biotic decay of birch bark could not be found in the literature.

Tree phellem cells that consist of suberized cells, such as birch cork, are understood to be very resistant to biological decay [35,36] because they are constructed to protect the plant/tree from infection by pathogen microorganisms [37]. Studies performed in the 1970s on the degradation of contemporary barks under natural burial conditions and in the laboratory reported that the phellem was the last component affected by fungi [38]. The decay was reported to start after 3 years of exposure, and microorganisms grew within the thick secondary tangential suberized cell walls. The growth of hyphae mechanically damages the cells by creating oval cavities, and this might lead to weight loss. Early studies on conifer barks showed that the weight loss caused by fungi in bark was five times smaller than that in wood, and that despite a weight loss of up to 10%, the physical properties may remain unchanged [39]. Several authors have shown that enzymes produced by fungi can degrade suberin [40–44], but the detailed pathways are still largely unknown, because suberin is strongly cross-linked and an unchanged extraction was not possible until new extraction techniques were developed [45,46]. Martins et al. [47] revealed that cutinasen, lipases and long-chain alcohol-modifying enzymes released by *Aspergillus nidulans* fungus depolymerises suberin. The long-chain fatty acids are broken down via peroxisomal β -oxidation. A very recent publication found that auxin-regulated GDSL lipases could degrade suberin [48]. Studies of enzymes from cold Arctic [49] and Antarctic [50,51] environments show that enzymes are active at temperatures close to 0 °C. Some enzymes have limited function, but activity at 0–15 °C is common for many of them [52].

Regarding archaeological wood, it is known that when it is recovered from low-oxygen sediments or under water, bacteria are the main cause of slow degradation [53–55], and

when it is exposed to air, fungi lead to a very fast metabolism controlled by temperature and humidity [56,57]. The absence of water and oxygen and low temperatures inhibit biotic decomposition, and changes due to chemical and physical processes may become evident [58]. However, very extreme conditions are required for microbial degradation to be completely suppressed [59]. Studies of wood biodegradation from Arctic regions have shown that predominantly soft rot is found [60,61], while brown rot plays a minor role and white rot could not be unequivocally identified [62]. It is an open question whether similar patterns of biotic decay are present in archaeological birch bark.

2. Materials and Methods

The morphology of birch bark has been examined visually, with light microscopy (LM) and transmission electron microscopy (TEM). In order to describe the decay of archaeological birch bark, the characteristics of contemporary non-degraded mature birch phellem was first investigated and compared with the characteristics of contemporary decayed in-nature phellem. The morphology of 13 samples from ice-logged, waterlogged and in-cave recovered archaeological birch barks was then investigated (Table 1).

2.1. Samples

The reference bark was a mature birch phellem collected from a felled *Betula pendula* tree about 30 years old in the district of Vex (Valais, Switzerland) in November 2014 (Figure 2). The naturally decayed bark was harvested from a fallen tree about 15 years old in Borgne Valley, Valais (Figure 3). The trunk was weathered in nature, laying on a sandy subsoil with stones. The fragment was chosen for its pronounced biological degradation, visible macroscopically as green, grey and brown-black staining, deposits and cracks. Such degradation was present especially at the lenticels and the inner bark (Figure 3). The ice-logged samples were taken from the Neolithic bow case from the Schnidejoch ice patch, Switzerland (Figure 4), and from three birch bark fragments retrieved from the Lendbreen ice patch, Norway (Figure 5). The Schnidejoch bow case has been described in a number of publications [63–65]. This object is dated to around 2800 BC and consists of three parts, a lid and an upper and lower body, that were found under different circumstances and in different conditions. Each part is made of 2 to 3 layers of superimposed outer birch bark strips sewn together with lime bast. The lid was subjected to a harmful ethanol treatment that extracted most of the alcohol-soluble components from the bark. It is now stored dry at ambient temperature. The upper and lower body are both untreated and stored damp and frozen at $-26\text{ }^{\circ}\text{C}$. The three Lendbreen birch bark fragments were found in a retreating ice patch located at the northern slope of Lomseggen ridge, Oppland (Norway). The ice patch extends from 1690 to 1920 m a.s.l. and the finds are dated between 300 and 1500 AD, with an accumulation of finds around 1000 AD [66]. The waterlogged sample was extracted from a Neolithic birch bark retrieved in Lake Moossee in Switzerland (521 m a.s.l.) during an excavation in 2011 (Figure 6). The layer from which the bark was retrieved dates between 4500 and 3800 BC. Since excavation, this bark, which was originally not harvested but detached naturally from a tree, as the phloem is still attached to the bark, is stored in distilled water at $4\text{ }^{\circ}\text{C}$. The last fragment (Figure 7) was recovered from a cave named Kosackenbergr, in the Kyffhäuser mountains west of Bad Frankenhausen in Germany and excavated in the 1950s. It is dated to the Bronze Age (2300–1800 BC) and, after unburial, has been preserved untreated in a sealed container.

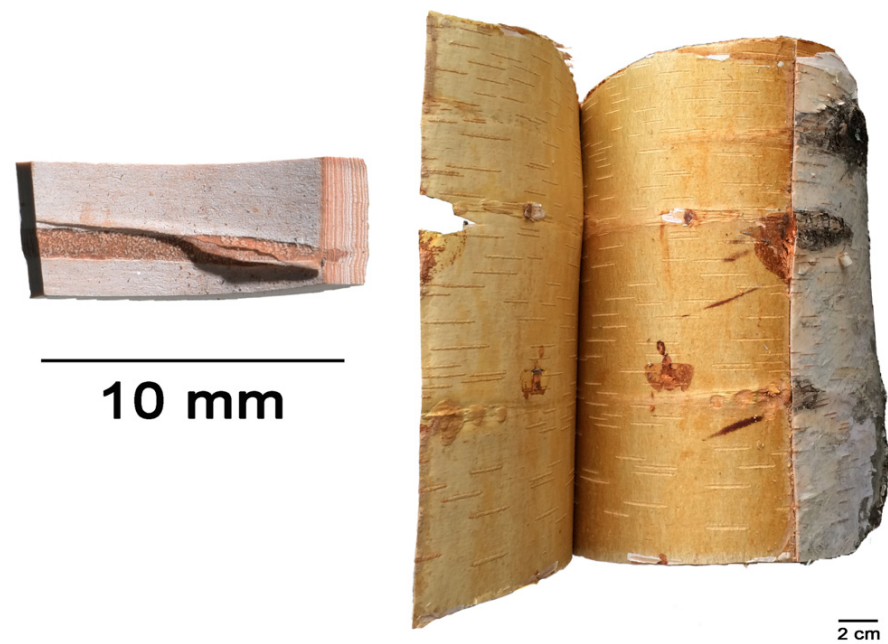


Figure 2. Reference sample (left) was extracted from contemporary outer birch bark harvested from a mature tree with strong and pliable phellem (right). Sample has white powdery surface due to betulin content and slight delamination is present at the lenticel. Thick- and thin-walled cell bands are recognizable macroscopically as red and white bands, respectively, along the radial section.



Figure 3. Birch bark fragment harvested from fallen trunk degraded in nature. Outer surface, especially when in contact with the ground, shows green, grey and brown discoloration and vertical cracks. Lenticels have cracks and overlays and are areas no longer clearly defined. On the inner side, remains of brittle and brown-black stained phloem are present and black circular deposits indicate areas of increased degradation. Location of analysed sample 0 is indicated with red rectangle.



Figure 4. (a) Lower and (b) upper part of Schnidejoch bow case body, ground-facing side; (d) upper part, upward facing. Samples were taken from outer bark strips (1, 6, 7), middle bark strips (2) and inner lining (3, 4, 8). Outer and middle bark strips of bow case body have outer bark surface oriented towards inside, and inner lining has outer bark surface oriented towards outside. Sample 4 was extracted from a fragment probably from (c) lid inner lining. Sample 5 was a loose fragment found close to the lower part (not shown).



Figure 5. Left: Lendbreen fragments; right: analysed samples. Sample 9 was taken from a weathered fragment; lenticels were fully eroded but sample was not brittle. Surface and cambium side were grey and faded. Cut surface was dark brown with a few reddish-brown areas. Sample 10 was taken from a rolled birch bark fragment, stiff but not brittle, with delaminated areas and large cracks. Cambium side (outer side in image) was compact and with a light, mainly grey-brown and white colour. Some holes from insect damage were present and normally elevated lenticels were recessed. On cut surface, outer layers were grey-brown, and only inner layers still exhibited original red-brown colour. Sample 11 was taken from a long narrow strip rolled on one end. Fragment was very strong, hard to cut and still pliable. Surface was weathered, coloured matte whitish-grey; red and brown colours were missing. Cut surface revealed unaltered colours in inner layers and grey outer layers.

Table 1. Analysed samples and their location, dating and burial conditions.

Sample	Object	Location	Date	Burial Conditions		
				Environment	T, RH	O ₂
Ref	Intact phellem	Valais, CH	Contemporary	tree		Ambient
0	Rotten phellem	Valais, CH	Contemporary	In-nature rotten tree		Ambient
1	Bow case, lower body	Schnidejoch	≈2800 BC (2905–2622 cal BC)	Ice patch	0 °C, 100% (*)	Low
2	Bow case, lower body	Schnidejoch	≈2800 BC (2905–2622 cal BC)	Ice patch	0 °C, 100%	Low
3	Bow case, lower body	Schnidejoch	≈2800 BC (2905–2622 cal BC)	Ice patch	0 °C, 100%	Low
4	Bow case, probably from lid	Schnidejoch	≈2800 BC (2881–2579 cal BC)	Ice patch	0 °C, 100%	Low
5	Bow case, lower body	Schnidejoch	≈2800 BC (2905–2622 cal BC)	Ice patch	0 °C, 100%	Low
6	Bow case, upper body	Schnidejoch	≈2800 BC (3011–2668 cal BC)	Ice patch	0 °C, 100%	Low
7	Bow case, upper body	Schnidejoch	≈2800 BC (3011–2668 cal BC)	Ice patch	0 °C, 100%	Low
8	Bow case, upper body	Schnidejoch	≈2800 BC (3011–2668 cal BC)	Ice patch	0 °C, 100%	Low
9	Fragment	Lendbreen	≈500 AD (430–540 cal AD)	Ice patch	−3 °C (**)	Low
10	Fragment	Lendbreen	≈900 AD (891–981 cal AD)	Ice patch	−3 °C	Low
11	Fragment	Lendbreen	≈1450 AD (1430–1470 cal AD)	Ice patch	−3 °C	Low
12	Fragment	Lake Moossee	4500–3800 BC	Waterlogged	≈4–16 °C (†)	Anoxic
13	Fragment	Kosackenbergl	2300–1800 BC	Cave	4–7 °C, ≈95% (‡)	Ambient

* [67], ** [68], † [69], ‡ [30].



Figure 6. Left: birch bark fragments from Lake Moosee (521 m a.s.l.) were recovered during an excavation in 2011 from a waterlogged sediment. Small, waterlogged fragments floating on water retain phloem, indicating that they were not harvested from the tree but detached naturally. During cutting, many fractures occurred, and small pieces broke off. Right: sample 12 does not have original white colour apart from a fresh fracture with splintered surface. Inner bark has dark-brown colour and is very brittle, and lenticels are not well defined and have frayed edges.



Figure 7. Sample 13 was extracted from a birch bark fragment recovered in the Kosackenberc cave. Inner and outer surfaces have reddish-brown overlay with white blooming. Normally alternating white and reddish-brown layers are not present, as reddish-brown colouring of thick-walled cells is completely lost. Lenticels have also lost their normally dark colour and are hardly distinguishable from normal phellem. Fragment is very light and extremely fragile; handling leads to fragmentation and loss.

2.2. Description of Embedding and Sectioning

Samples 1–3, 6–8 and 12 were wet, while the others were already air-dried. They were all documented and cut with a razor blade to a rectangular size of about 7 mm × 3 mm. The cutting provided information about the brittleness and risk of delamination. First attempts showed that non-embedded sectioning did not allow for a thorough study of deterioration due to the separation of the layers during cutting. Further, the lumen content of the thin-walled cells obscured the cell wall study and had to be removed [25]. After test staining with safranin aniline blue, toluidine blue, a polychromatic stain commonly used to highlight fungal structures in plant cells walls [70] or to examine erosion bacteria degradation in waterlogged wood [71], was used.

Thin sections were obtained by immersing the samples in 70, 80 and 96% ethanol (Alcosuisse, Switzerland) and twice in 100% ethanol (Merck, Darmstadt, Germany) for at least 3 h each at room temperature. The samples were then immersed twice in 100% acetone (Merck, Darmstadt, Germany) for at least 2.5 h at room temperature and in increasing concentrations of Epon/acetone solution (1:2, 1:1, 2:1). Finally, they were embedded in 100% Epon (Fluka, Switzerland) and left to harden at 60 °C for 5 days.

Thin sections of 1 µm were produced for LM with a UC6 ultramicrotome (Leica Microsystems, Vienna, Austria) and put on glass slides with 1 mL of distilled water. The glass slides were placed on a hot plate with a temperature of 55 °C to stretch the sections. After evaporating the water, they were stained with an aqueous solution of 0.5% toluidine blue O (*w/v*) (Merck, Darmstadt, Germany) for 3 min at 55 °C. They were then washed in water, dried on the hot plate and mounted with Entellan[®] (Merck, Darmstadt, Germany).

Ultrathin sections (75 nm) were cut from the same embedded samples for electron microscopy (TEM). The sections, mounted on 200 mesh copper grids, were stained with Uranylless (Electron Microscopy Sciences, Hatfield, PA, USA) and lead citrate (Leica Microsystems, Vienna, Austria) with an ultrastainer (Leica Microsystems, Vienna, Austria).

2.3. LM and TEM

The permanent slides were investigated with an Olympus BH-2 light microscope using transmitted and polarized light at different magnifications (04×, 10×, 40×, 60×). Photographs were taken with a Jenoptik ProgRes SpeedXT digital camera. If needed, Helicon Focus 6 stacking was used to produce a fully focused image.

TEM ultrathin sections were examined with a transmission electron microscope (CM12, Philips, Eindhoven, the Netherlands) equipped with a digital camera (Morada, Soft Imaging System, Münster, Germany) and image analysis software (iTEM). ImageJ was used to quantify dimensions in the sections.

3. Results

The micromorphology of cell structure and degradation was investigated on transverse and radial sections. To facilitate the comparison among the results, mostly radial sections are shown in this paper.

We first present a careful description of the micromorphology of the reference material and the contemporary bark decayed in nature, followed by an analysis of the 13 archaeological samples. The morphological features were systematically described, and 13 degradation characteristic patterns were identified and named with abbreviations to facilitate their localisation on the LM and TEM images (Table 2). For each feature, example LM and TEM images are presented. Macroscopic images of the samples are shown in the previous section. The occurrence of degradation features in the samples is summarized in a table.

Table 2. Occurrence of degradation features in samples. x indicates the feature was present in the analysed sample. Fractures, unfolding of thin-walled cells and hyphae are also present in the reference material, a piece of contemporary intact birch bark.

	Fra	Un	No-bi	In-st	Swe	Ir	Det	Rem	Re-th	Hy	Vo	Me	Acc
Ref	x	x								x			
0	x	x	x	x-fu	x-fu	x	x-fu-wl	x-fu	x-fu	x	x-fu	x-fu	
1		x	x	x-fu	x-fu		x-fu-cl	x-fu	x-fu			x-fu	
2	x	x	x	x-ov	x-fu		x-fu-cl	x-fu		x			
3	x	x	x		x-ov	x	x-ov			x (rarely)			
4	x	x, x-st			x-ov, x-fu	x	x-ov-wl, x-fu-cl	x-fu					
5		x					x-ov-wl, x-fu-cl	x-ov					
6	x	x	x	x-fu	x-fu		x-wl-fu x-fu-cl	x-fu	x-fu	x	x-fu	x-fu	
7	x	x	x	x-fu	x-fu		x-fu-wl	x-fu		x	x	x	
8	x	x	x	x-ov	x-ov	x	x-ov	x-ov					
9	x	x						x-ov, x-fu		x (rarely)			
10	x	x		x-ov	x-fu, x-ov			x-ov, x-fu		x	x-fu		
11	x	x			x-fu			x-fu		x	x-fu		
12	x	x	x	x-ov	x-ov		x-fu?-wl, x-fu?-cl	x-fu?		x (rarely)	x-ba	x-ba	
13	x	x	x	x-ov	x-fu		x-fu-wl	x-fu		x (rarely)			x

The following features may be associated with fungi or bacteria, or overall in the sample. To distinguish among these cases, the suffix fu (fungi), ba (bacteria) or ov (overall) is added to the abbreviation:

- Fra: Fracture of radial cell walls;
- Un: Unfolding of compressed thin-walled cell; if it is in conjunction with stretching of the thick-walled cells, it is marked as Un-st;
- No-bi: Absence of birefringence of secondary wall of thick-walled cell;
- In-st: Intense toluidine blue staining;
- Swe: Swelling and/or disaggregation of the secondary cell walls;
- Ir: Increased irregularity of cell shape and size leading to irregular cell arrangement;
- Det: Detachment, either of cells from each other (Det-cl) or secondary cell walls from the compound middle lamella (Det-wl) or the tertiary wall;
- Rem: Removal of phenolic compounds in the lumen of thick-walled cells or the compound middle lamella or in the secondary cell walls;
- Re-th: Reduced cell wall thickness;
- Hy: Hyphae in thin-walled cell lumen;
- Vo: Circular/oval voids in the corners of secondary thick-walled cell walls with a diameter of about 0.6 μm , or smaller voids in the secondary cell walls with diameter of about 1.2 μm aligned along or in the compound middle lamella; the former are

caused by mechanical penetration in the wall by hyphae, the latter by the penetration of bacteria;

- Me: Complete dissolution of cell structure;
- Acc: Accumulation of foreign substance in the cell lumen of thin-walled cells.

3.1. Reference Material: Contemporary Intact Birch Bark

The bark morphology of the reference sample was examined with light microscopy (Figure 2). The radial thin sections revealed a compactly arranged and regular cell structure consisting of an equal number of thin-walled and thick-walled cell bands, with the former being more hydrophilic than the latter (Figure 8). The thin-walled cells were heavily compressed in the outer portion of the bark but originally had a square shape, visible in the centre of the radial thin section. The shape of the lumen varied and was generally lenticular. The compound middle lamella and tertiary walls had a deeper blue colour than the secondary walls, an indication of their greater affinity for water [12]. The barely coloured thick-walled cell walls, on the other hand, showed strong birefringence. Suberin had a crystalline structure showing birefringence [72].

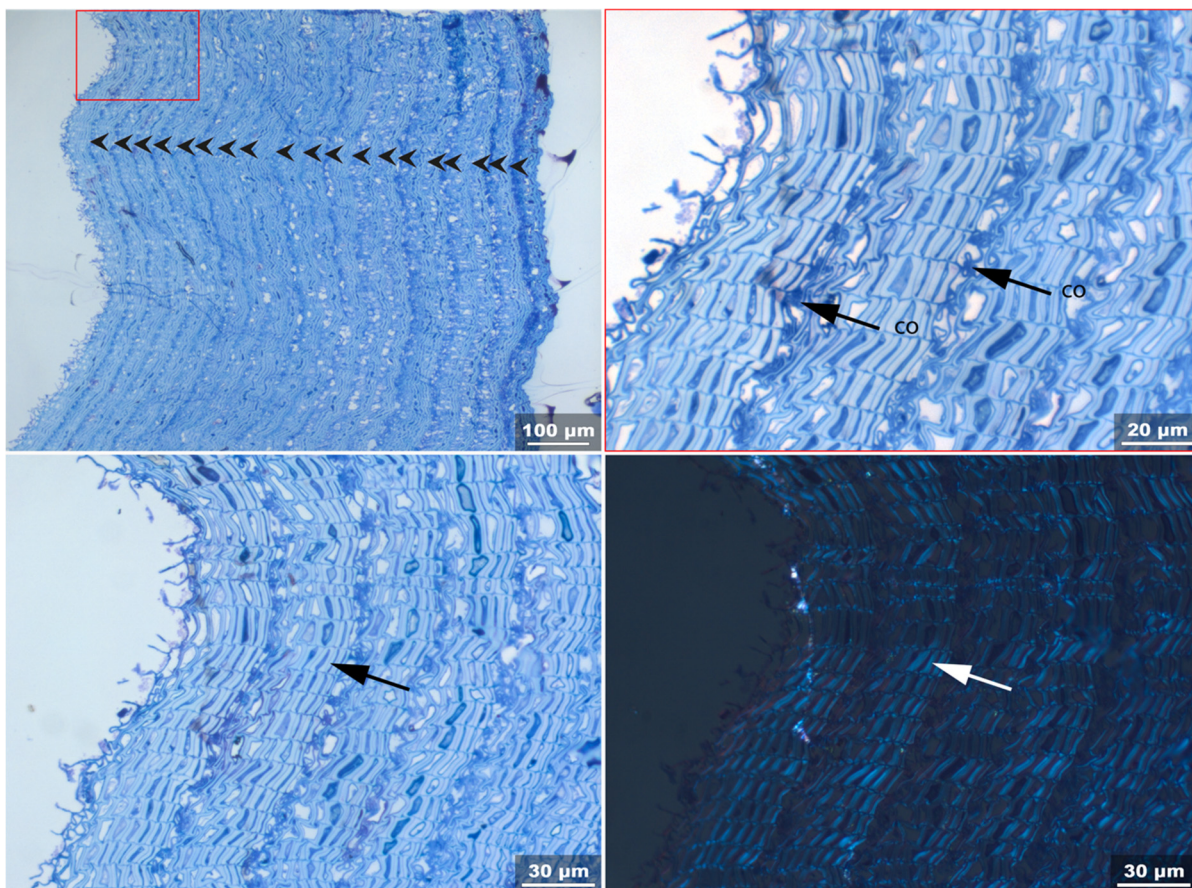


Figure 8. Reference sample. LM images of radial thin sections (**left**, outer surface; **right**, inner side) reveal thick-walled and thin-walled cell bands (arrowheads, **top left**). Tips of arrows indicate boundaries between thin-walled and thick-walled cell bands. Compressed thin-walled cells are marked with “co” (**top right**). Water affinity of thin-walled cell walls, compound middle lamella and tertiary walls can be appreciated from the intensity of blue staining. Thick-walled cell walls are hydrophobic (light blue) and show strong birefringence (**bottom, left and right**). Sample shows overall strong birefringence of thick-walled cells. While thin-walled cells usually have only very weak birefringence, the birefringence of thin-walled cell layer at boundary with thick-walled cells is just as strong as that of thick-walled cells.

The TEM investigation of the reference sample shows the arrangement of cells and the layered structure of cell walls (Figure 9). In the thick-walled cell bands, the radial

compound middle lamella was about $0.24 \pm 0.03 \mu\text{m}$ thick with a net-like structure in the centre and dark rims. The tangential compound middle lamella was $0.08 \pm 0.01 \mu\text{m}$ thick and electron dense, an indication of higher lignification [73,74]. Interruptions in the tangential compound middle lamella were present. At the transition between the thick- and thin-walled cell bands, the radial compound middle lamella built a thick corner with ends susceptible to fracture. The thick-walled cells were filled with electron-dense compounds with an irregular shape. In the thin-walled cell bands, it was not possible to distinguish between radial and tangential compound middle lamella, as the cells were compressed. The compound middle lamella had a homogeneous structure and was about $0.08 \pm 0.02 \mu\text{m}$ thick. The secondary wall is suberized, and therefore had a lamellar structure with very fine dark lines, arranged around dense globular particles. The tertiary wall is the boundary layer at the lumen and was very dense. The thin-walled cells were partly filled with a very dark multiform compound.

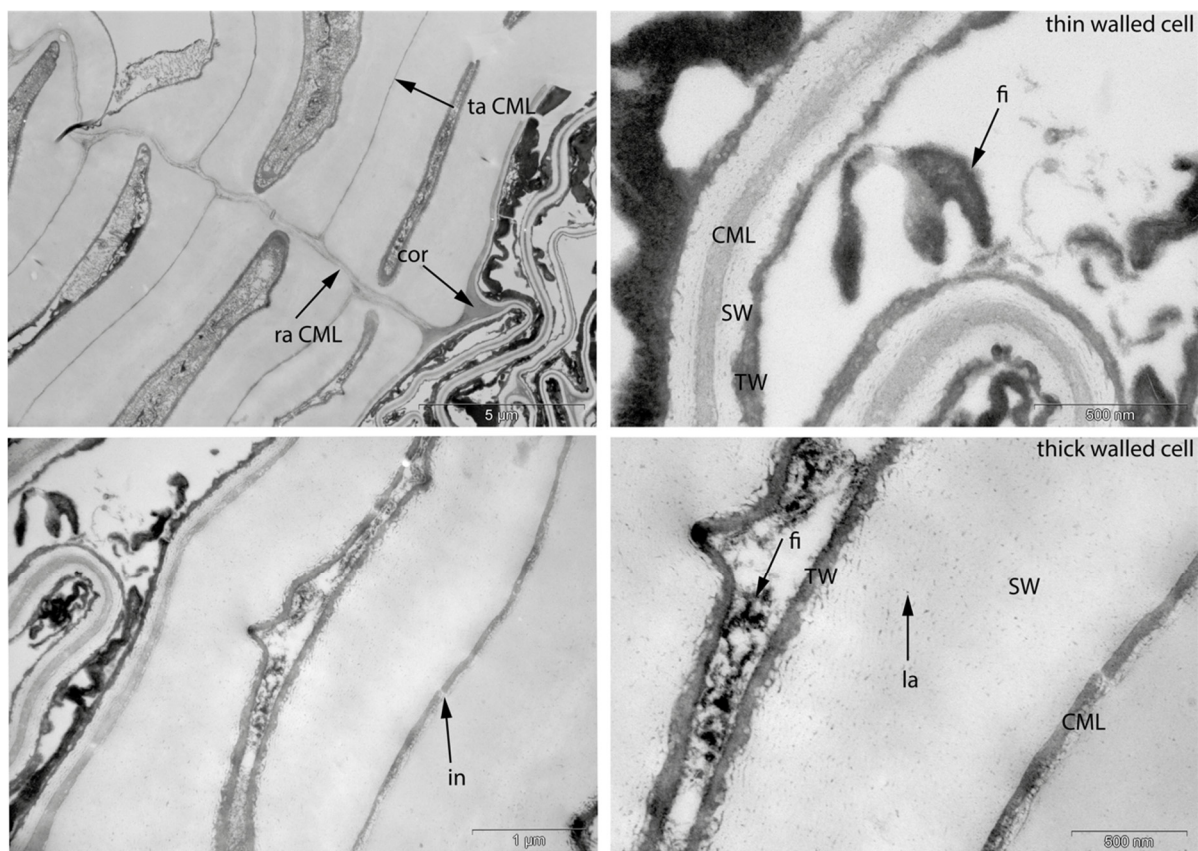


Figure 9. Reference sample. TEM images of thick-walled and thin-walled cells. The compound middle lamella (CML) is thicker in radial direction (ra) than tangential direction (ta) in thick-walled cell bands (**top left**). In tangential direction, interruptions of composite middle lamella are present (in, **bottom left**). There is a clearly pronounced corner (cor) at the transition between thick- and thin-walled bands. Details of thin-walled cell (**upper right**) and thick-walled cell (**bottom right**) are presented. SW, secondary wall; TW, tertiary wall; la, lamella of secondary suberized cell wall; fi, filling material.

Close to the lenticel, the reference sample was delaminated (Figure 2, left). LM images show that separation of the layers occurred at the boundary between thin- and thick-walled cell bands. Fracture occurred in the radial thin-walled cell walls (Figure 10, left). The consequence was a tangential separation (delamination) of the layers and the unfolding of thin-walled cells. The dark blue and purple balls and bubbles and the pinkish cloudy structures visible on the outermost layers of the toluidine-stained radial thin sections indicate the presence of hyphae. TEM images of the same area show fungal structures in the lumen of the cells and a hypha penetrating from one cell to another.

The breakthrough has thin dark coloured edges, an indication that the cell wall was altered by enzymatic degradation.

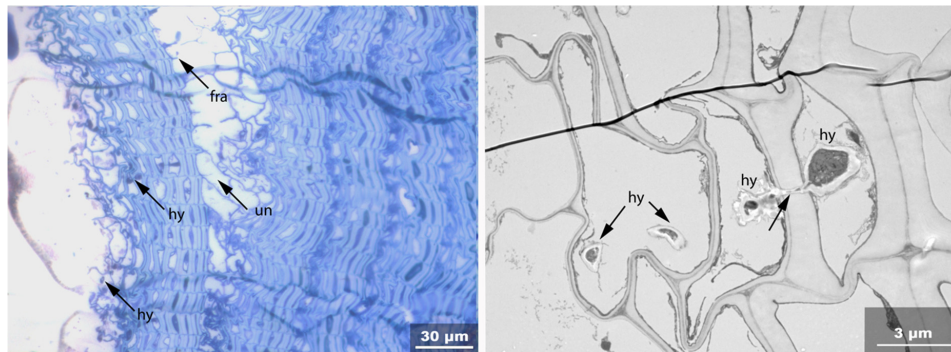


Figure 10. Reference sample. LM images (**left**): delamination due to breaking of boundary radial cell walls (fra) accompanied by unfolding of compressed thin-walled cells (un). TEM images (**right**): hyphae within thin-walled cell lumen and penetrating all wall layers.

Figure 11 shows a lenticel. Lenticels are fanned out layers with a convex shape, more pronounced towards the phloem. Proceeding tangentially from the normal phloem to the lenticel, the thick-walled cell bands form a continuous structure. The transition between normal phloem and lenticel involves about 4–5 cells where the cell lumen of the thick-walled cells changes from a square to ellipsoid shape, while the walls of the thin-walled cells become heavily fractured. The radial cohesion of the thick-walled cells has numerous failures. The remains of the fractured thin-walled cells are strongly stained, an indication of their highly hydrophilic nature. The thick-walled cells display no birefringence in the centre of the lenticels, while this increase approaching the transition to the normal phellem.

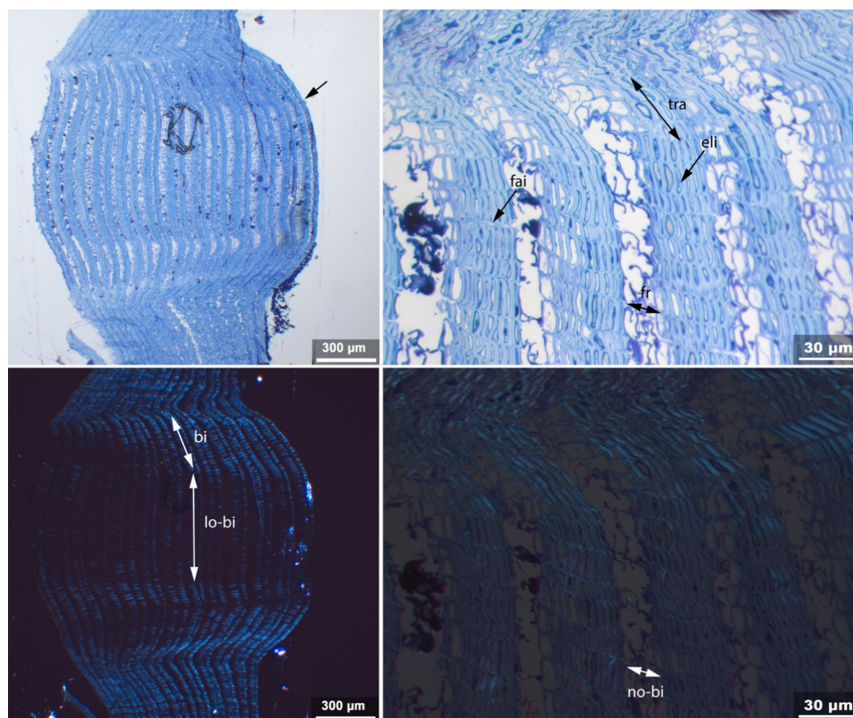


Figure 11. Reference sample. Lenticel with fanned out thick-walled bands (**top left**). Detailed image of cell structure (**top right**) shows ellipsoid lumen (eli) of thick-walled cells and fractures (fr) of thin-walled cells. Birefringence of thick-walled cells is low at lenticel centre (lo-bi, **bottom left**) and rises at the transition to normal phellem (bi), while it is absent in thin-walled fractured cells (no-bi, **bottom right**).

TEM images (Figure 12) show that within the tangential thick-walled cell walls of the lenticel, plasmodesmata about 25 to 30 nm in diameter are present. They are unbranched and have a tubular shape, and they connect two cells. They are filled with electron-dense material, and occasionally a deposit is visible on the inner surface of the cell. In the lenticel, small intercellular spaces can be found, while they are absent in the normal phellem.

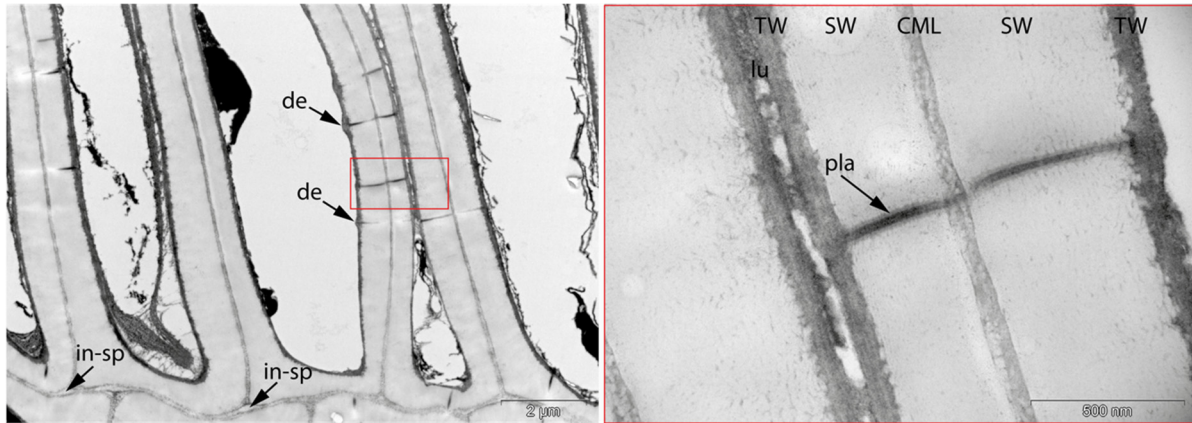


Figure 12. Reference sample. TEM images of thick-walled cell of lenticel with plasmodesmata (pla) in tangential wall and intercellular spaces (in-sp) in radial cell corners. Tubular plasmodesmata are filled and occasionally have a deposit (de) towards the cell lumen.

3.2. Sample 0: Contemporary Birch Bark Degraded in Nature

This sample presents all identified degradation features except for decay by bacteria and the accumulation of foreign substances, which was present only in sample 13, retrieved from a cave environment.

In the LM pictures, it is possible to identify degraded areas characterized by unfolding of the thin-walled compressed cells and an irregular arrangement of the cell structure. Birefringence is strongly present in the well-preserved areas, whereas it is completely missing in the degraded areas. All layers of thick-walled cells are visible in the well-preserved areas (Figure 13). The toluidine staining is stronger on the suberized secondary cell walls and weaker on the compound middle lamella. The phenolic compounds in the cell lumen are absent.

The penetration of the secondary wall by hyphae caused circular voids located at the cell corners. Further, swelling and loosening of the wall is visible, leading to complete secondary wall disintegration. Finally, only a dark blue unstructured substance remains. Hyphae are visible in the lumen of the cells, leading to decay in parts of the tertiary walls (Figure 14, bottom left and top right).

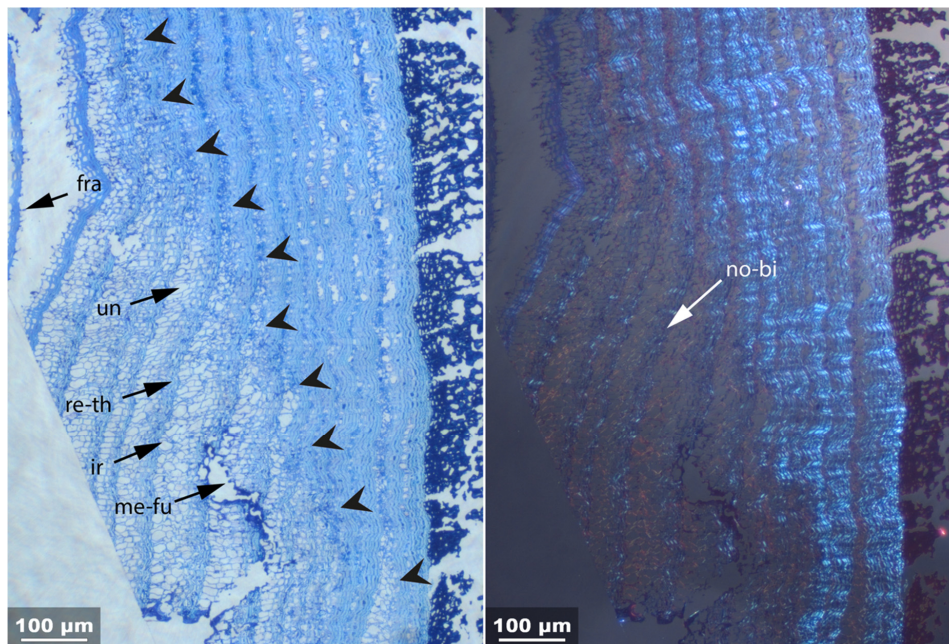


Figure 13. Sample 0. LM overview under transmitted light (left) and polarised light (right). Arrows on the left mark transitions between differently preserved areas. Degraded areas are characterized by unfolding of thin-walled cells (un), increased irregularity of cell arrangement (ir) and reduction of cell wall substance, especially suberized secondary wall of thick-walled cells (re-th) up to complete dissolution of cell structure (me-fu). Fracture of thin radial walls and layer separation are also visible (fra). In degraded area, thick-walled cells do not show birefringence (no-bi).

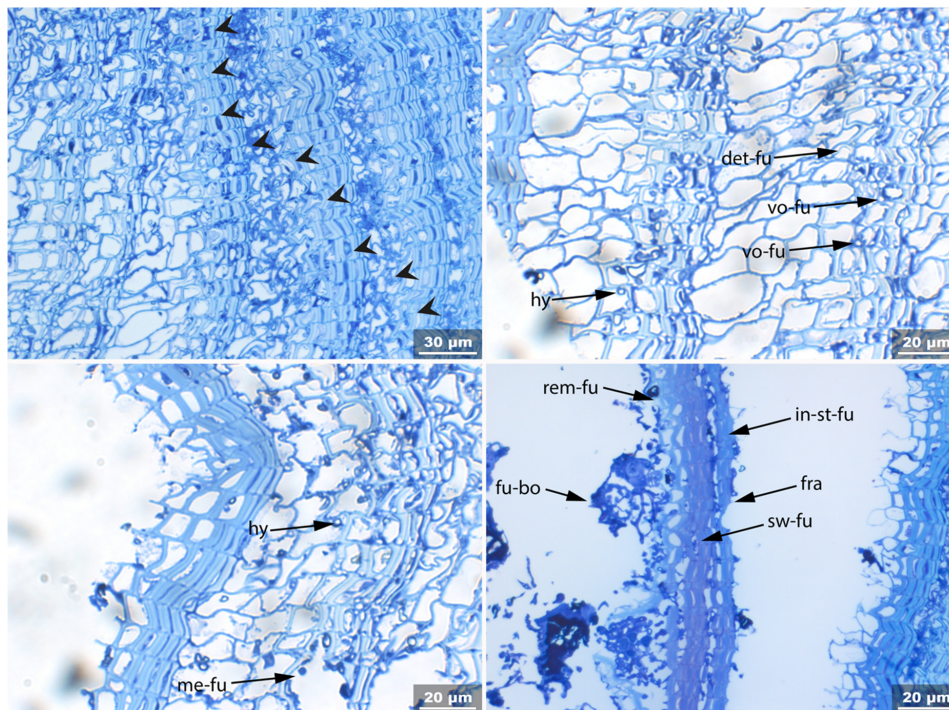


Figure 14. Sample 0. LM overview of sample with clear boundary between well-preserved area and fungal degraded area (arrowheads). Secondary walls of thick-walled cells are penetrated mainly in the corners by hyphae (vo-fu), and hyphae are present in thin-walled cell lumen (hy). These adhere to the tertiary cell wall and sometimes cause it to detach (det-fu) (top right). At bottom left, complete dissolution of cell structure is visible (me-fu). At bottom right, fungal structures can be seen (fu-bo). These cause a decrease in lignin-containing middle lamella (rem-fu) and phenolic lumen filling of thick-walled cells. At the same time, darker staining (in-st-fu) and swelling of secondary cell wall occur (sw-fu). Fractures due to breaking of radial thin-walled cells (fra) are also visible.

The TEM pictures show that the secondary cell walls, which are infested with hyphae in the corners, causing oval voids, are swollen, their structure is loosening and their shape is irregular (Figure 15). Advanced degradation is indicated by disintegration of the wall; in some cases the cell wall seems to be completely digested, while in others an electron-dense granular residue is left. Similar compounds have been identified in sclereid of beech bark in the area around the hyphae, and interpreted as remnants of not completely degraded lignin [75]. Connected to the infestation with hyphae, the phenolic compounds in the lumen, compound middle lamella and secondary walls were removed (Figure 16). This led to separation of the cells along the compound middle lamella.

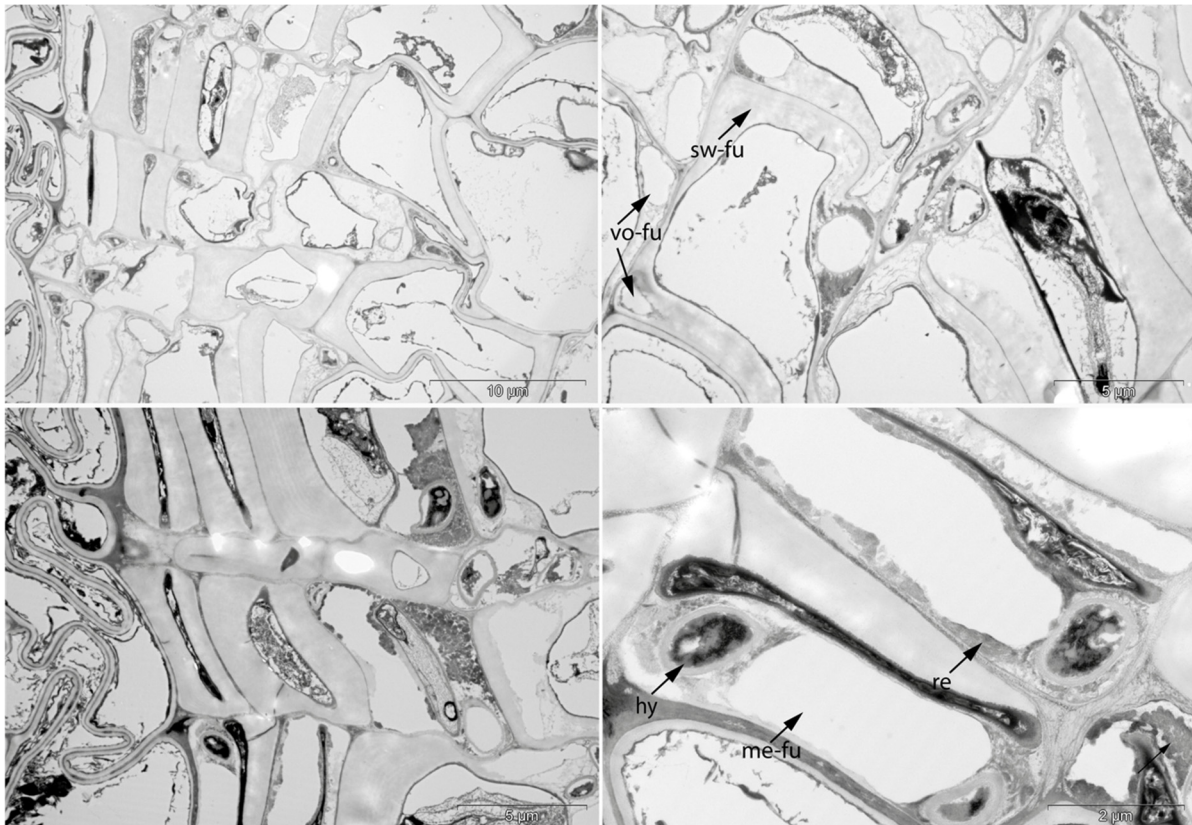


Figure 15. Sample 0. TEM images illustrating degradation feature called circular voids. At top right, empty cavities not filled with hyphae are visible (vo-fu). In the same picture, swelling and loosening of secondary cell wall can be seen (sw-fu). At bottom right, cells with corners penetrated by hyphae (hy) are visible. These have almost completely metabolised the suberised wall, leaving only a little granular dark residue (re).

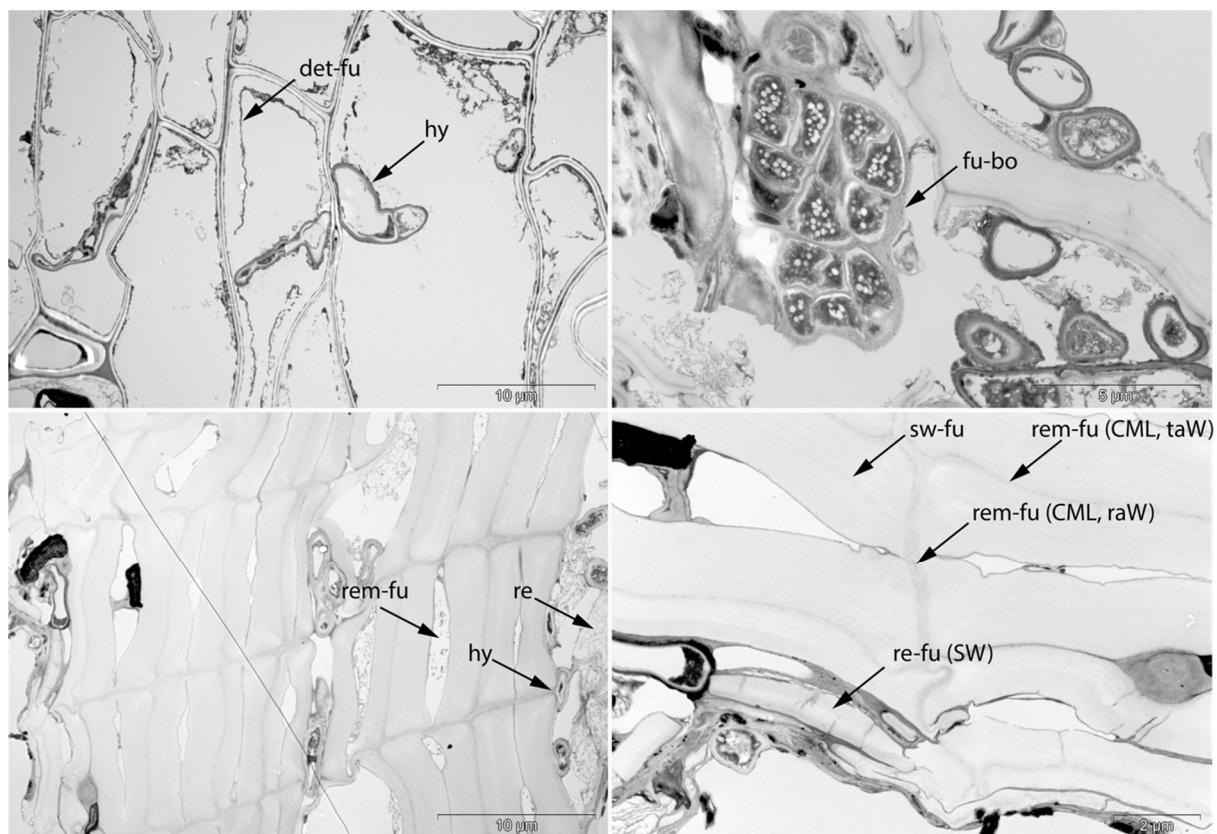


Figure 16. Sample 0. TEM images. **Top left:** hyphae (hy) in thin-walled cells and partial detachment of tertiary cell wall layer (det-fu). **Top right:** fungal body (fu-bo) and hyphae in thick-walled cell bands caused removal of lignin from middle lamella (rem-fu, CML) (**bottom right**) and phenolic content from cell lumen (rem-fu) (**bottom left**). Suberised cell wall swelled and lost narrow lamellae, an indication of suberisation (sw-fu). Wide light and dark bands appear, and in an advanced stage of degradation, the thickness of the wall is reduced (re-fu, SW).

3.3. Archaeological Samples

3.3.1. Sample 1

In the archaeological samples, the presence of biotic decay was macroscopically visible by surface discoloration. Swelling of the cell walls, removal of substance and increased staining were commonly found microscopic features of biotic decay. One example is provided by a dark discoloured area on sample 1, extracted from the lower body of the Schnidejoch bow case on the ground-facing side (Figure 4, top left). The cut section of the sample had a brown colour with alternating white betulin-filled bands and showed no delamination or breaking-off pieces due to the cutting process. LM images reveal a very heterogeneous preservation condition. The area marked 1 in Figure 17 is characterized by an intact regular cell structure with compressed thin-walled cells and slight birefringence of the thick-walled cells. The blue coloration of the secondary cell walls is slightly darker compared to the reference material. The area marked 2 is located at the surface of the sample and is characterized by the presence of fungi. The effect of fungi can be observed in both LM and TEM images. They cause swelling and disintegration of the suberised cell walls (Figure 17), which acquire a dark blue colour upon staining and exhibit no birefringence. Further, fungi cause degradation of the compound middle lamella, reducing its thickness (Figure 17). Finally, the cells are detached and the phenolic filling material in the thick-walled cells are degraded (Figure 17).

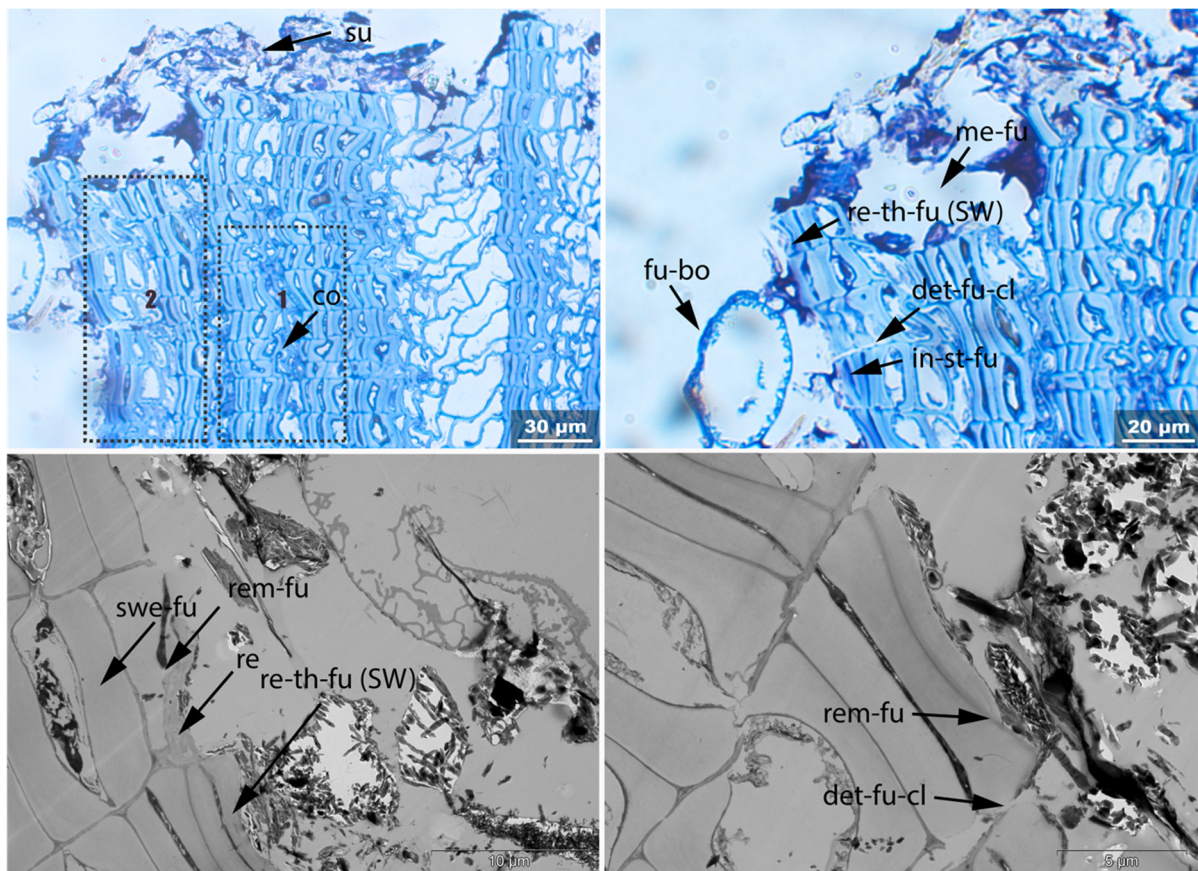


Figure 17. Sample 1. Top left: LM image of thin section. Area 1 has very well-preserved cell structure; area 2 is biodegraded. Superficial deposits are visible (su). In area 1, thin-walled cells are still compressed (co) and secondary cell wall layer of thick-walled cells is still birefringent (not shown). In area 2, clear change is noticeable in secondary cell wall layer: dark blue staining (in-st-fu), swelling (swe-fu) and dissolution of the wall (re-th-fu). Middle lamella (rem-fu) is also degraded (rem-fu), eventually leading to radial detachment of cells (det-fu-cl) (top right). Cavity in upper area (top right) between superficial and cell structure can be seen, in which complete cell structure dissolution occurred (me-fu). Changes to cell walls can be seen in more detail in TEM: thick-walled suberised cell walls are clearly swollen and loosened (swe-fu), after which they lose thickness (re-th-fu, SW), leaving unstructured residue (re). Phenolic content of cell lumen is also degraded (rem-fu) (bottom left). Alterations of compound middle lamella can be seen at bottom left; wall loses thickness and electron density area is reduced (rem-fu).

3.3.2. Sample 2

Fractures and unfolding of the compressed thin-walled cells are particularly visible in sample 2. Sample 2 (Figure 18, top left) was extracted from the middle bark strips in a dark-brown discoloured area. The cut section showed delamination and breaking-off pieces due to the cutting process. LM images (Figure 18, top right) reveal strong tangential delamination due to the breaking of radial cell walls. The secondary cell walls of the thick-walled cells have a dark blue colour, an indication of higher water absorption. No birefringence of thick- and thin-walled cells was detected, and the thin-walled cells were no longer compressed (bottom left).

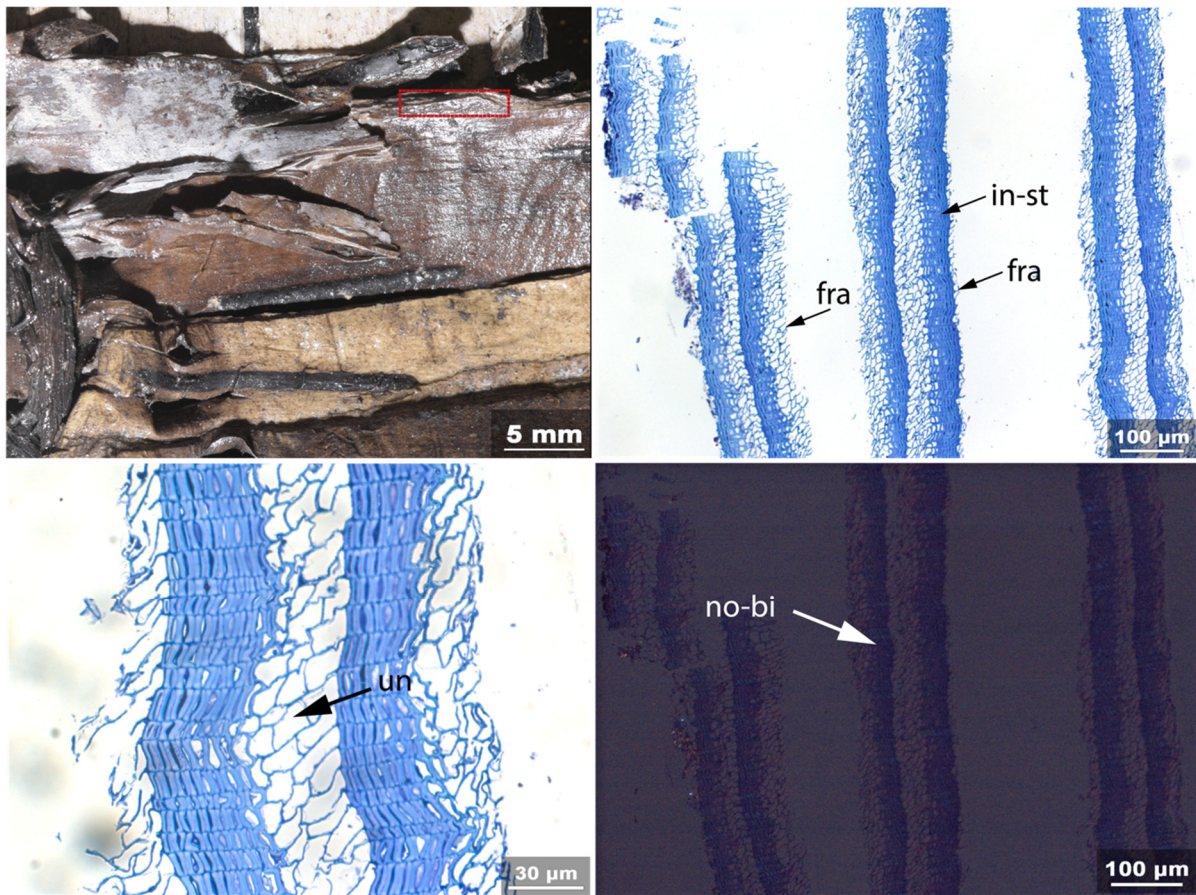


Figure 18. Sample 2. **Top left:** location of sample. **Right:** LM of thin sections. Tangential delamination is visible due to fracture (fra) of radial thin-walled cells. Increased toluidine staining of thick-walled cells is also appreciable (in-st). **Bottom left:** thin-walled cells in normal phellem are overall unfolded (un). **Bottom right:** birefringence is absent in both thick- and thin-walled cells.

3.3.3. Sample 3

Increased irregularity of the cell structure and detachments are particularly visible in sample 3. Sample 3 was extracted from the inner lining and contained a lenticel; no surface discolouration was present. LM images reveal that all cell wall layers were present, despite being swollen and irregular (Figure 19). In some areas the thin-walled cells were still compressed. Many broken radial cell walls at the boundary between thick- and thin-walled cell layers were present, but no complete delamination was detected. Slight fungal degradation was present on the left outer layer, which caused a dissolution of cell walls and a reduction in the middle lamella and phenolic compounds. Thick- and thin-walled cells displayed no birefringence.

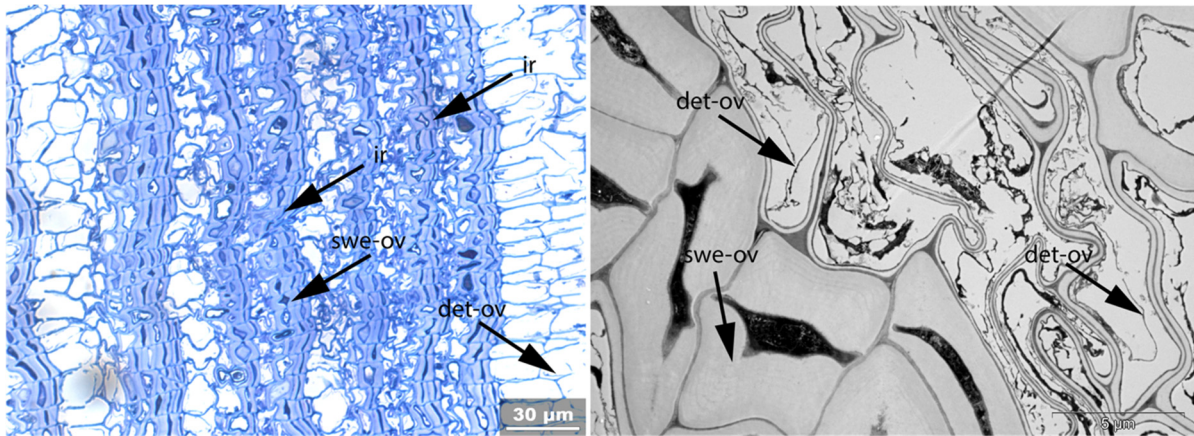


Figure 19. Sample 3. **Left:** LM image. Secondary cell walls of thick-walled cells are swollen (swe-ov). Deformation of cells has also taken place, leading to irregular structure (ir). Parts of tertiary cell wall of thin-walled cells are detached (det). **Right:** TEM image. Swelling of secondary cell wall of thick-walled cells is visible, together with detachment of parts of tertiary cell wall of thin-walled cells. In sample 3, this phenomenon is widespread and not localised.

3.3.4. Sample 4

A further degradation feature is the detachment of the secondary cell wall from the compound middle lamella and the tertiary wall. This is visible in sample 4. Unfolding of thin-walled cells and stretching of thick-walled cells is also present. Sample 4 was taken from the bow case inner lining, but the original position on the object is unknown, possibly the lid. The birch bark is slightly pliable and retains some strength. The surface is compact but shows cracks and delamination in the top half (Figure 4c). The bark is somewhat brittle, especially the lenticel. The outer side of the bark is grey, the inner brown. In the lower area, a black cloudy discoloration is visible that is also present on the edges. Red-brown colours are strongly reduced.

Thin section 4a shows a higher degree of decay than 4b. This sample is characterized by unfolding of thin-walled cells, elongation in the transverse direction of thick-walled cells and increased staining. Along with this, the structure becomes irregular. While in sample 4b the cell structure is regular, the walls of the thin-walled cells are still slightly folded and there is only slight light blue staining of the secondary cell walls, an indication of low water sorption.

The detachment of the secondary cell wall from the compound middle lamella and the tertiary wall affected large areas of thin section 4a and only slightly affected thin section 4b (Figure 20). TEM images (Figure 21, bottom right) show that due to this separation, voids and threadlike structures appear between the wall layers. The very thin, delaminated tertiary cell wall layer is present as a ring within the lumen. The swelling of the secondary cell wall causes a wave deformation of the secondary wall layer. The compound middle lamella is broken, and interruptions are present. The original structure of the suberin lamella has disappeared and broad light and dark bands with the same orientation as the former suberin lamella have formed. The degradation of the compound middle lamella led to a separation of the cells and a degradation of the phenolic content, visible as reduced cell lumen content.

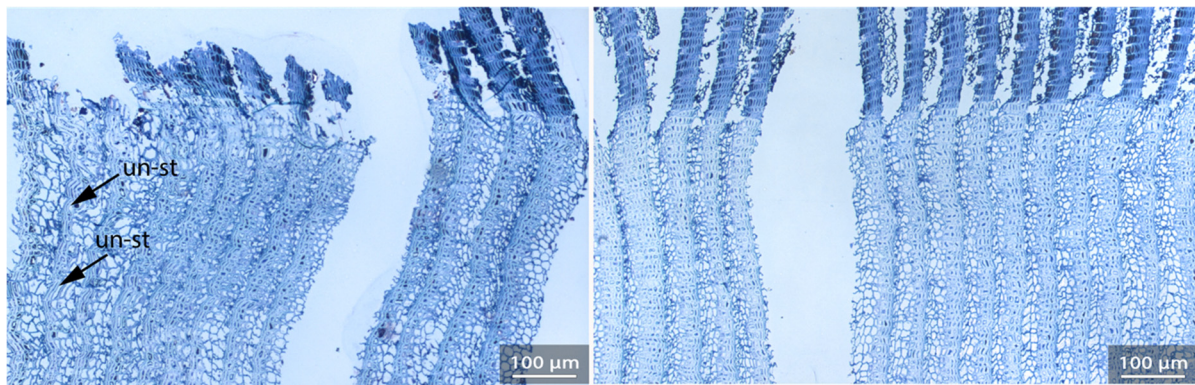


Figure 20. Sample 4. Two thin sections, about 4 mm apart, were made from the embedded sample: thin section 4a (left) and thin section 4b (right). Thin section 4b reveals a much better-preserved cell structure than 4a: it is regular, walls of thin-walled cells are still slightly folded and there is only slight light blue staining of secondary cell walls, an indication of low water sorption; thin section 4a shows unfolding of thin-walled cells and stretching of thick-walled cells (un-st).

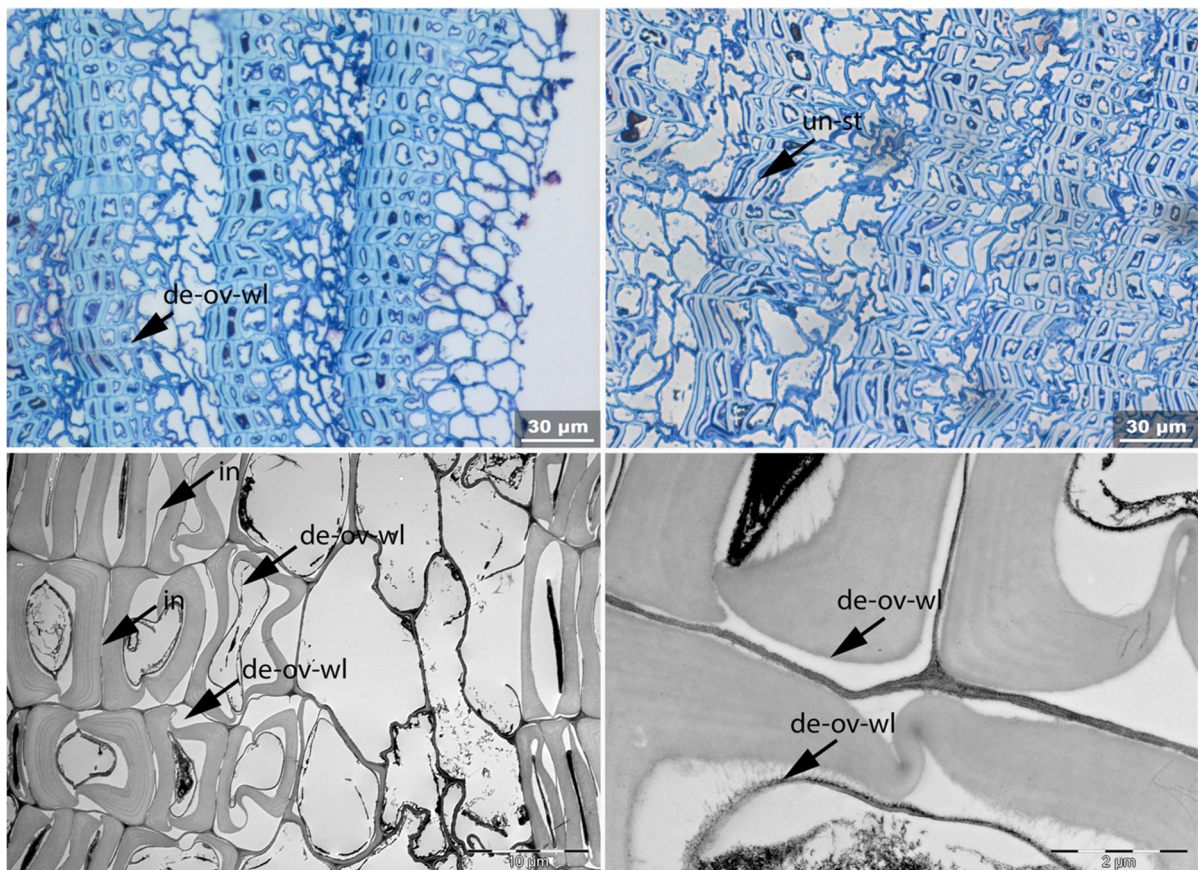


Figure 21. Sample 4a. Detachment of secondary cell wall from compound middle lamella is found throughout (de-ov-wl, top left). Elongation of thick-walled cells (un-st) is present (top right). TEM (bottom left) shows detachments of secondary wall from compound middle lamella and tertiary wall (de-ov-wl). Very thin, delaminated tertiary cell wall layer is present as a ring within the lumen. Compound middle lamella is broken and shows large interruptions (in). Swelling caused wave deformation of secondary wall layer. Separation and threadlike structures appear between secondary and tertiary wall (bottom right). Original structure of suberin lamella has disappeared and broad light and dark bands with the same orientation as the former suberin lamella are formed.

3.3.5. Sample 6

Fungal degradation causes circular/oval voids in the secondary wall of thick-walled cells, and an advanced state of decay leads to complete dissolution of the structure (Figure 22). Both are found in sample 6, extracted from the upper part of the bow case body on the ground-facing side. The area where the sample was taken was fully exposed to the soil. All exposed surfaces showed discolouration macroscopically. The LM reveals strong fungal degradation starting from both exposed sides. The strongest degradation is found at the surface layers, and some of the innermost layers are not affected. The circular voids are mainly located in the corners and were caused by the penetration of hyphae. In contrast to the decayed in-nature sample 0, the remains of hyphae in the holes are no longer present in sample 6. In an advanced stage of decay, swelling of the secondary cell walls occurred, followed by their disintegration. The skeleton of the middle lamella was the last to be metabolised. A superficial structure that consists of cell fragments, fungal structures and cloudy, dark blue parts remains on the sample surface.

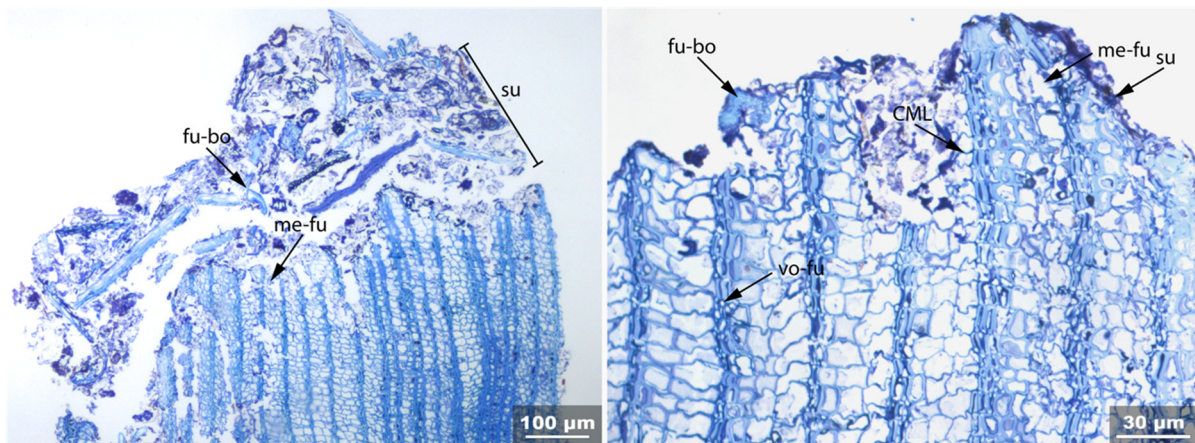


Figure 22. Sample 6 shows a superficial structure (su) consisting of cell fragments, fungal structures (fu-bo) and dark blue cloudy remains (left). Empty circular/oval voids in corners (vo-fu) of suberized cell walls of thick-walled cells caused swelling and then dissolution of secondary wall (right). At top of sample, complete disintegration of cell structure (me-fu) is visible. Fungal structures cause a loss of cell wall material (secondary cell wall, cell lumen filling material) and in an advanced state complete disintegration of all cell wall layers (me-fu).

3.3.6. Sample 10

A further degradation feature is the removal of phenolic cell wall components from all cell wall layers and cell lumen-filling substances, leaving behind a wall that is bleached but unchanged in thickness. This phenomenon was only found on the surface, up to 0.06 mm deep. An example is sample 10, extracted from a rolled birch bark recovered in permafrost in Lendbreen. Both surfaces were white-grey and lost the red-brown colour, which was retained in the inner layers (Figure 5). The bleaching involved the superficial five cell layers (Figure 23). The compound middle lamella, the secondary and tertiary walls and the cell lumen lost components that bind with the toluidine dye and cause birefringence. The thickness of the walls was unchanged, and no disaggregation of the structure occurred. After a transition of a few cell layers, in which the secondary cell wall was slightly swollen and more strongly stained, the deeper layers showed an unchanged appearance, birefringence was present to a large extent and the thin-walled cells were still compressed. Thick and thin-walled cells were stained with a similar blue tone, slightly darker than that of the reference material.

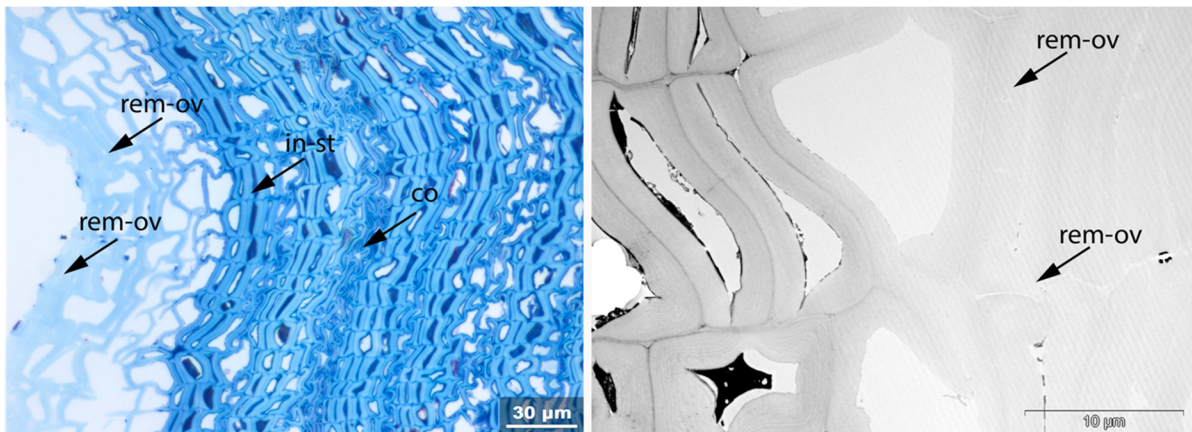


Figure 23. Sample 10. **Left:** LM. Loss of phenolic compounds from cell wall layers and lumen is visible in left outer bands (rem-ov). Deeper layers are unchanged and display birefringence (not shown). Thin-walled cell walls are compressed (co). In transition zone between bleached and unchanged phellem a slight swelling (swe) and increased blue staining (in-st) of secondary cell wall is visible. **Right:** TEM. Overall loss of phenolic components is significant and a change in appearance of the thin lamella structure of secondary cell wall is visible.

3.3.7. Sample 11

In some cases, fungal infestation can be clearly visible by the presence of hyphae within the lumen of thin-walled cells, but the cell structure retains regularity, birefringence and water-repellent properties. An example is sample 11, extracted from a pliable and considerably strong Lendbreen fragment. The colour of the fragment was grey-whitish matte with a weathered surface; red and brown colours were missing superficially but were retained in the inner part of the sample (Figure 5).

LM shows a very regular, compact birefringent structure that reflects a good preservation condition. The walls of thick-walled cells have a pale colour and are therefore still water-repellent (Figure 24, left). Round cavities in the secondary walls and hyphae are found within the lumen of thin-walled cells. The hyphae are arranged along the tertiary wall and appear to metabolise it or parts of it from the lumen (Figure 24, right). At the contact point between the hyphae and wall, the wall thickness is often reduced. It can be assumed that hyphae are able to mechanically break through cell walls, as otherwise they would not have been able to distribute themselves so extensively throughout the cell structure. However, the secondary cell wall and the composite middle lamella are not degraded over a wider area by this type of fungus.

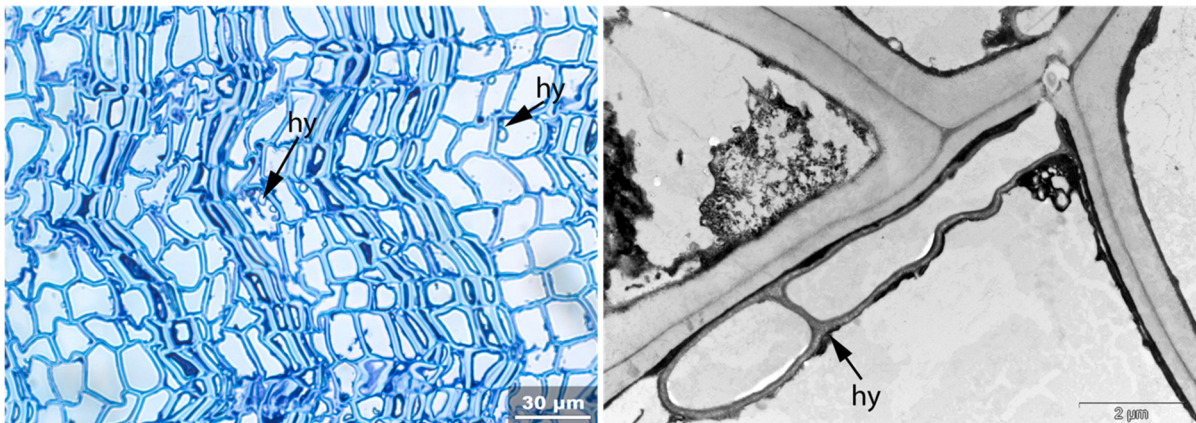


Figure 24. Sample 11. **Left:** LM. Hypha present in lumen of thin-walled cells distributed over entire thin section. Hyphae are aligned along tertiary wall and cause reduced thickness. **Right:** TEM. Division of hyphae into two cells (septum) is present. Defects are visible in a corner of the secondary cell wall and the middle lamella, possibly caused by hyphae.

3.3.8. Sample 12

The waterlogged sample found in anoxic sediment showed biotic degradation mainly by bacteria, and to a much lesser extent by fungi. Bacterial degradation was recognizable as many small voids in the secondary cell walls and complete metabolism of the cell structure. Macroscopically, the strength of this Neolithic sample was considerably reduced; many fractures occurred during cutting. Due to the waterlogged condition, the susceptibility to layer separation could not be determined. The bark can still be identified as birch bark, but the surface is brown.

LM thin sections (Figure 25) reveal a regular cell structure with un-folded and overall swollen thin-walled cells. Fractures in the radial thin cell walls are present in some areas, but complete delamination did not occur. The secondary walls show increased staining and no birefringence (not shown). The phenolic content in the thick-walled cells is still present and very dark in colour, sometimes fractured. The fracture (in a radial direction) sometimes affects not only the lumen filling substance, but also the wall. Detachments of cells along the middle lamella and of cell wall layers within individual cells are present (not shown).

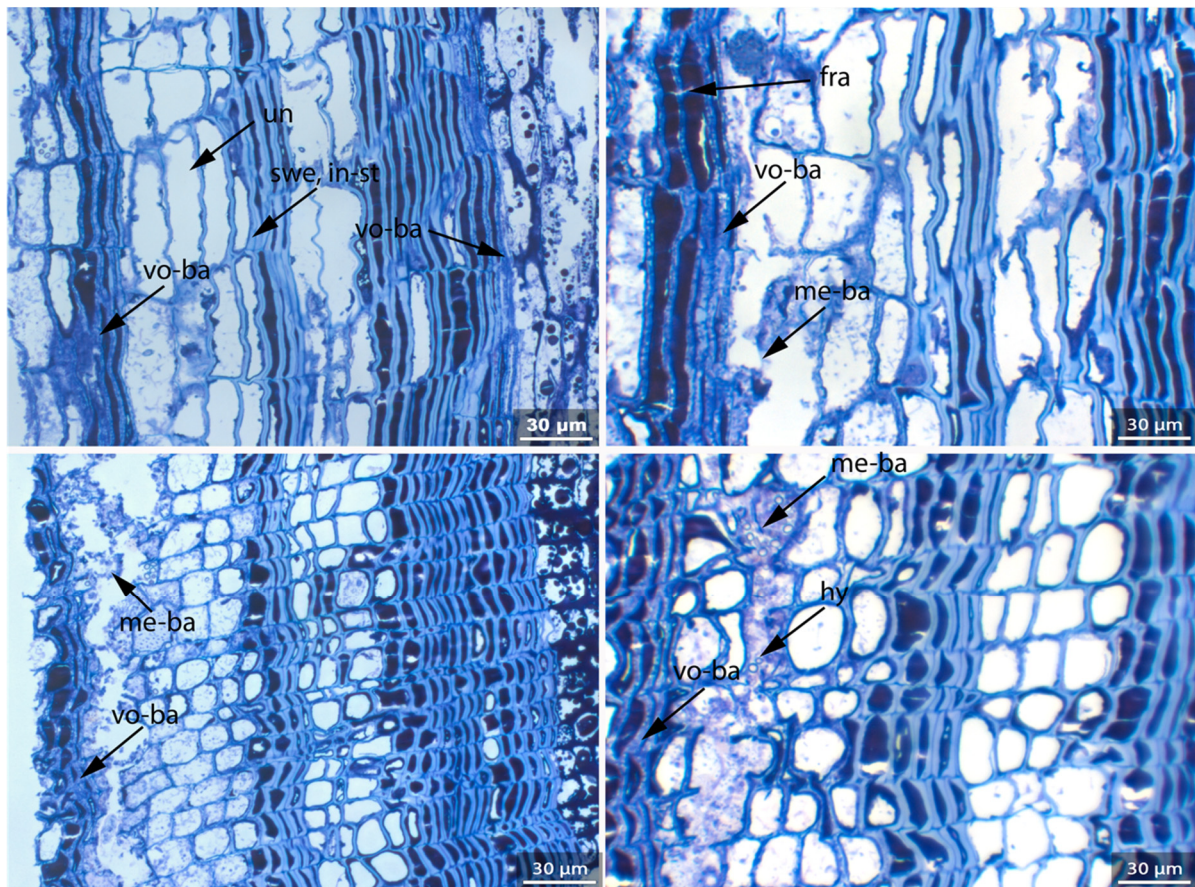


Figure 25. Sample 12. **Top left and right:** LM of cross-section. **Bottom left and right:** LM of radial thin section. Bacteria created voids (vo-ba) in secondary cell wall and, in advanced stage, metabolised all cell wall layers and phenolic lumen content of thick-walled cells (me-ba). Cloudy purple material was produced that accumulated in the lumen of thin-walled cells. Decay is strongest on sample surface, on left outer cell bands, indicating that bacteria penetrated from there. Few hyphae are found in the sample (hy). Entire sample shows increased staining (in-st), swollen cell walls (swe) and unfolded thin-walled cells (un). Radial fractures running across phenolic content and cell walls are present (fra).

The TEM examination showed that bacteria were mainly located in the secondary cell walls and were aligned along the middle lamella (Figure 26, right) and the tertiary wall, causing voids. Their location indicates that they metabolised carbohydrate-containing components of the compound middle lamella and the tertiary wall. In the advanced stage of degradation, the middle lamella and the phenolic components in the cell lumen of the thick-walled cells are also degraded. Based on the characteristic degradation traces, they can be identified as tunnelling bacteria [76].

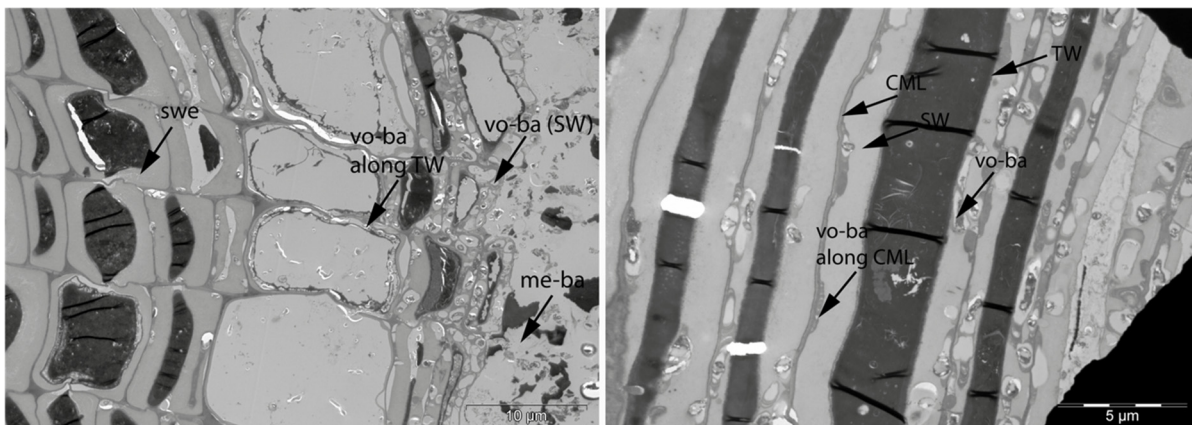


Figure 26. Sample 12. TEM: swelling and loosening of secondary walls of thick-walled cells (swe) and voids created by bacteria in secondary cell wall of thick- and thin-walled cells. Bacteria are aligned along compound middle lamella and tertiary wall, creating tunnels with concentric rings, characteristic of tunnelling bacteria. Based on the appearance, the presence of erosion bacteria is possible. Bacteria were able to digest all cell wall layers and phenolic lumen content (me-ba).

In addition to the biotic degradation, TEM sections show that the structure of the secondary cell wall has changed considerably: the wall is swollen, with broad light and dark stripes, and in some places, it is only preserved as a loose net with many defects. The cohesion of the cell wall layers is also greatly reduced, resulting in cell detachment (not shown).

3.3.9. Sample 13

The final degradation feature identified microscopically in the archaeological samples was the accumulation of foreign substances within the cell lumen. This was found in sample 13, recovered from the Kosackenber cave. Both inner and outer surfaces of the sample had a reddish-brown overlay, while the internal layers had a light, slightly pink colour and the normally white and reddish-brown alternating bands were no longer perceptible. White blooming was present on both surfaces. The reddish-brown colouring of the thick-walled cells was completely lost. The lenticels lost their normally dark colouring and were hardly distinguishable from normal phellem. The sample was extremely fragile, and handling caused the loss of small fragments. The cohesion of layers was very reduced (Figure 7).

LM reveals a regular structure with several fractures of radial cell walls and complete layer separations (delamination). The thin-walled cells are unfolded, and increased staining of the thick secondary cell walls is visible; the closer to the surface, the darker the shade of blue. Over the entire thin section, a thick, dark-coloured, partially birefringent residue is visible on the surface (Figure 27). Furthermore, purple-blue cloudy material is found in the lumen of the thin-walled cells. It can be assumed that this is gypsum, as this was identified in analyses of birch cork from the same site [30]. As gypsum is poorly soluble in water, it is assumed that the ions were dissolved in water and then precipitated inside the cells and accumulated in the lumen. The phenolic content of the thick-walled cells is strongly reduced. In the cell layers near the surface, sporadic hyphae are found. Furthermore, close to the phloem, the secondary cell walls of thick-walled cells are extremely swollen or absent (not shown).

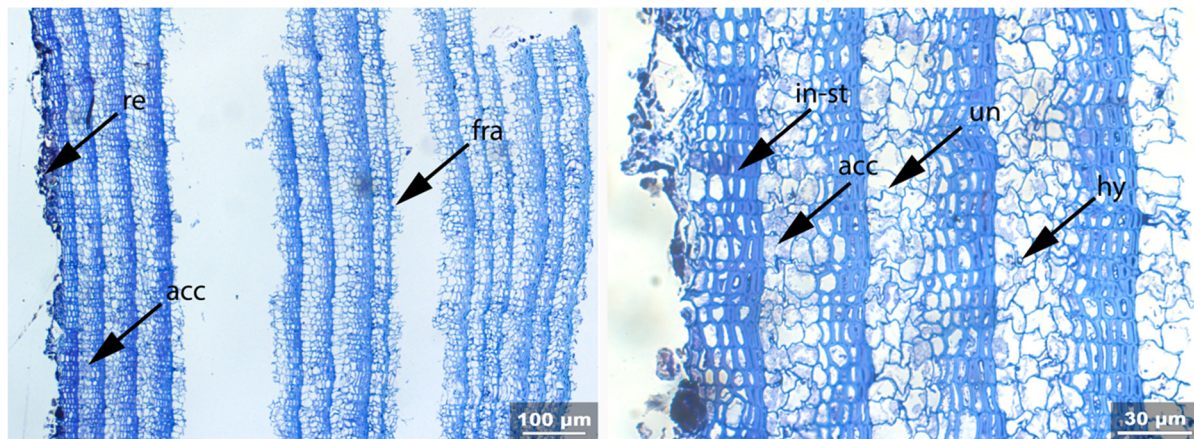


Figure 27. Sample 13. LM shows many fractures of radial thin-walled cells (fra) leading to delamination. Thin-walled cells are unfolded (un); thick-walled secondary cell walls reveal increased staining, especially close to the surface. Thick dark-coloured residue (re) covers the surface. An accumulation of a cloudy substance in the lumen of thin-walled cells (acc) is present; some lumens are completely filled.

4. Discussion

The identification and systematic description of microscopic degradation features and the macroscopic characteristics such as colour, brittleness and pliability of the 15 birch bark samples analysed in this study allowed us to establish a correlation between some macroscopic and microscopic features.

If delamination was macroscopically visible, fractures and detachments of thin-walled cell walls were found. If the sample surface showed discoloration, decay at a microscopic level was found. Bacterial decay was only found in the waterlogged sample, while fungal decay was common. However, if biotic decay is very localised, it might not lead to macroscopic colour changes. If the samples were exposed to sunlight, they lost their red-brown colour and appeared strongly weathered, and removal of the phenolic compounds from the cell walls and lumen could be found in the very outer layers. However, it was not possible to establish a correlation between macroscopic brittleness and microscopic degradation features. For example, the Lendbreen samples are macroscopically strongly weathered but microscopically intact, except for the outer layers. Similarly, the Kosackenberg sample is macroscopically extremely brittle, but microscopically all the cell wall layers have been preserved. Microscopic biotic decay might be present in well-preserved and pliable samples such as our contemporary reference sample. More importantly, the occurrence of microscopic degradation features is very local in birch bark and can vary within the same fragment.

The next step in interpreting the collected microscopic data was to try to establish any causality for the identified degradation features. Clearly, the presence of hyphae as well as voids in the cell walls, and the reduction in cell wall thickness and the complete disintegration of cells are all connected to biotic decay, mostly fungal, except for the waterlogged sample, in which bacteria were found. Biotically produced enzymes can also lead to the swelling of cell walls, removal of phenolic compounds, reduction in wall thickness and detachment of cells from each other or from the compound middle lamella [77], but in this case, these features were restricted to areas close to the hyphae. When the loss of phenolic compounds is present overall but confined to the upper layers, and when macroscopically the surface has lost its brown-red colour, photocatalysis of the phenolic compounds due to sunlight has probably taken place [23,78]. Irregularity of the cell structure and, consequently, the cell arrangement, swelling of the cell walls, increased toluidine blue staining and loss of birefringence can also be found in the absence of signs of biotic decay, and we suggest that they are due to chemical degradation of the cell walls. In particular, loss of birefringence can be connected to a loss of crystallinity of

suberin [72,79]. Toluidine blue staining, though, is not selective for suberin, and a thorough investigation of suberin degradation should be performed using different methods.

Accumulation of foreign substances, probably gypsum, was only detected in the fragments recovered from the cave environment and might be due to the deposition of salts dissolved in the water the samples were exposed to. Finally, fracturing and unfolding of thin-walled cell walls and elongation of thick-walled cell walls are mechanical degradation features that might have chemical, biotic or physical causes. In particular, unfolding of thin-walled cells has been detected in combination with every degradation feature and is a reliable microscopic degradation marker. Unfolding has been found in other phellem samples upon exposure to solvents or heat [9,80]. The age of the samples did not correlate with the state of preservation, at either the macroscopic or microscopic level.

5. Conclusions

Careful examination of sections of 15 samples of birch bark, two contemporary and 13 archaeological, using light and electron transmission microscopy, allowed us to provide, for the first time, a comprehensive description of microscopic degradation features of birch bark and correlate with macroscopic visible features. Further, we could establish causes for a number of these features. Understanding the correlation between macroscopic and microscopic features is essential in order to develop passive or active conservation measures. The most important macroscopic features that allow us to predict the microscopic state of the samples' preservation are colour changes, such as surface discolorations and loss of the red-brown colour, and changes in mechanical properties, such as a loss of pliability, presence of delamination and increased brittleness. Colour changes and delamination may be connected to microscopic features, and a microscopic analysis can trace whether they are caused by biotic, chemical or physical decay. The most relevant microscopic feature that was detected in association with every degradation form was unfolding of thin-walled cells. This is therefore a reliable microscopic degradation marker. However, the increased brittleness could not be connected to a specific microscopic feature and would need to be assessed macroscopically, for example by quantifying the loss of fragments while handling or cutting the samples. Future research should concentrate on understanding possible causes for the increased brittleness of some birch bark archaeological objects, establishing whether there are correlations with the burial environment, and developing remedial measures specific to such objects.

Author Contributions: J.K. and G.D.P. conceived this study. J.K. prepared samples and performed the LM and TEM and analysed the images. J.K. interpreted the degradation and prepared images. G.D.P. was responsible for funding acquisition and project administration. J.K. and G.D.P. wrote the paper. All authors have read and agreed to the published version of the manuscript.

Funding: This research was funded by the Swiss National Science Foundation (SNSF), grant number 159662 (<http://p3.snf.ch/Project-159662>, accessed 20 July 2021).

Institutional Review Board Statement: Not applicable.

Informed Consent Statement: Not applicable.

Data Availability Statement: The datasets used and/or analysed during the current study are available from the corresponding author on reasonable request.

Acknowledgments: The authors would like to thank Jostein Bergstøl and Jörg Hägele-Masnick for the kind donation of archaeological birch bark samples; Thomas Volkmer, Gaspard Clerc, BFH Biel, Robertas Ursache, and Fritz Schweingruber, WSL Zürich, for testing cutting, embedding and staining methods on birch bark; Paul Saffo for the preparation of orthophotos from the bow case used in Figure 4, and Nadim Scherrer for technical support in microscopy. A special thanks to Beat Haenni, University of Bern, for the skilled embedding and sectioning of the samples. The authors also would like to thank Adriano Boschetti, Archaeological Service of the Canton of Bern, and Albert Hafner, University of Bern, for support of the "Unfreezing History" project.

Conflicts of Interest: The authors declare no conflict of interest. The funders had no role in the design of the study; in the collection, analyses, or interpretation of data; in the writing of the manuscript; or in the decision to publish the results.

References

1. Lüttge, U.; Kluge, M.; Bauer, G. *Botanik*; Wiley Verlag: Weinheim, Germany, 2005.
2. Kost, B. Die Gewebe der Gefäßpflanzen. In *Strasburger-Lehrbuch der Pflanzenwissenschaften*; Kadereit, J.W., Körner, C., Kost, B., Sonnewald, U., Eds.; Springer: Berlin/Heidelberg, Germany, 2014; pp. 72–96.
3. Chang, Y.-P. *Anatomy of Common North American Pulpwood Barks*; Technical Association of the Pulp and Paper Industry: Tokyo, Japan, 1954.
4. Jensen, W. The Connection between the Anatomical Structure and Chemical Composition and the Properties of Outer Bark of White Birch. *Pappers-och trävarutidskrift för Finl. Suom. Pap.-ja Puutavaraalehti* **1949**, *15*, 113–119.
5. Jensen, W.A. *Botanical Histochemistry: Principles and Practice*; Freeman, W.H.: San Francisco, CA, USA, 1962; Volume 12.
6. Evert, R.F.; Esau, K.; Langenfeld-Heyser, R.; Eichhorn, S.E. *Esau's Pflanzenanatomie: Meristeme, Zellen und Gewebe der Pflanzen- ihre Struktur, Funktion und Entwicklung*; Walter de Gruyter Verlag: Göttingen, Germany, 2009.
7. Klügl, J.; Hafner, A.; Di Pietro, G. On the rolling and plasticization of birch bark (in print). In Proceedings of the 14th ICOM-CC Wet Organic Archaeological Materials (WOAM) Working Group Conference, Portsmouth, UK, 20–24 May 2019.
8. Fortes, M.A.; Rosa, M.E. Growth stresses and strains in cork. *Wood Sci. Technol.* **1992**, *26*, 241–258. [[CrossRef](#)]
9. Krahmer, R.L.; Wellons, J.D. Some Anatomical and Chemical Characteristics of Douglas-Fir Cork. *Wood Sci.* **1973**, *6*, 97–105.
10. Xu, X.; Schneider, E.; Zaremba, C.; Stucky, G.D.; Wudl, F. Modification of the Semitransparent Prunus serrula Bark Film: Making Rubber out of Bark. *Chem. Mater.* **1998**, *10*, 3523–3537. [[CrossRef](#)]
11. Groh, B.; Hübner, C.; Lenzian, K. Water and oxygen permeance of phellem isolated from trees: The role of waxes and lenticels. *Planta* **2002**, *215*, 794–801. [[CrossRef](#)] [[PubMed](#)]
12. Schönherr, J.; Ziegler, H. Water permeability of Betula periderm. *Planta* **1980**, *147*, 345–354. [[CrossRef](#)] [[PubMed](#)]
13. Shibui, H.; Sano, Y. Structure and formation of phellem of Betula maximowicziana. *Int. Assoc. Wood Anat.* **2018**, *39*, 18–36. [[CrossRef](#)]
14. Zajączkowska, U. Cork. *eLS* **2016**, 1–8.
15. Mauseth, J.D. *Botany: An Introduction to Plant Biology*; Jones & Bartlett Learning: Burlington, MA, USA, 2019.
16. Pinto, P.; Sousa, A.; Silvestre, A.; Neto, C.P.; Gandini, A.; Eckerman, C.; Holmbom, B. Quercus suber and Betula pendula outer barks as renewable sources of oleochemicals: A comparative study. *Ind. Crop. Prod.* **2009**, *29*, 126–132. [[CrossRef](#)]
17. Ekman, R. The Suberin Monomers and Triterpenoids from the Outer Bark of Betula-verrucosa Ehrh. *Holzforschung* **1983**, *37*, 205–211. [[CrossRef](#)]
18. Jensen, W.; Fremer, K.E.; Sierilä, P.; Wartiovaara, V. The Chemistry of Bark. In *The Chemistry of Wood*; Browning, B.L., Ed.; Interscience Publishers: New York, NY, USA; London, UK, 1963.
19. Ferreira, J.P.A.; Quilhó, T.; Pereira, H. Characterization of Betula pendula Outer Bark Regarding Cork and Phloem Components at Chemical and Structural Levels in View of Biorefinery Integration. *J. Wood Chem. Technol.* **2017**, *37*, 10–25. [[CrossRef](#)]
20. Koljo, B.; Sitte, P. Das Suberin. In *Die Chemie der Pflanzenzellwand: Ein Beitrag zur Morphologie, Physik, Chemie und Technologie der Cellulose und ihrer Begleiter*; Treiber, E.E., Ed.; Springer: Berlin/Heidelberg, Germany, 1957; pp. 416–432.
21. Kiyoto, S.; Sugiyama, J. Histochemical structure and tensile properties of birch cork cell walls. *Cellulose* **2021**. [[CrossRef](#)]
22. Graça, J.; Santos, S. Suberin: A Biopolyester of Plants' Skin. *Macromol. Biosci.* **2007**, *7*, 128–135. [[CrossRef](#)] [[PubMed](#)]
23. Tse, S.; Dignard, C.; Kata, S.; Henderson, E.J. A study of the light sensitivity of birch bark. *Stud. Conserv.* **2018**, *63*, 423–440. [[CrossRef](#)]
24. Monahan, V. *Condition of Artifacts from Ice Patches*; 2008.
25. Klügl, J.; Hafner, A.; Di Pietro, G. Towards a description of the degradation of archaeological birch bark. In Proceedings of the ICOM-CC 18th Triennial Conference Preprints, Copenhagen, Denmark, 4–8 September 2017.
26. Orsini, S.; Ribecchini, E.; Modugno, F.; Klügl, J.; Di Pietro, G.; Colombini, M.P. Micromorphological and chemical elucidation of the degradation mechanisms of birch bark archaeological artefacts. *Herit. Sci.* **2015**, *3*, 1–11. [[CrossRef](#)]
27. Vasiljeva, N. *Softening, Drying and Consolidation of Birch Bark*; 2018.
28. Klügl, J.; Di Pietro, G. The interaction of water with archaeological and ethnographic birch bark and its effects on swelling, shrinkage and deformations. *Herit. Sci.* **2021**, *9*, 3. [[CrossRef](#)]
29. Fletcher, L.; Milner, N.; Taylor, M.; Bamforth, M.; Croft, S.; Little, A.; Pomstra, D.; Robson, H.K.; Knight, B. The Use of Birch Bark. In *Star Carr Volume 2: Studies in Technology, Subsistence and Environment*; Milner, N., Taylor, B., Conneller, C., Eds.; White Rose University Press: York, UK, 2018; pp. 419–534.
30. Hägele-Masnick, J. The birch bark torches from the Kyffhäuser caves. In Proceedings of the 13th ICOM-CC Group on Wet Organic Archaeological Materials Conference, Florence, Italy; 2016; pp. 392–394.
31. Larsen, P.K.; Jensen, L.A.; Ryhl-Svendson, M.; Padfield, T. The microclimate within a Neolithic passage grave. In Proceedings of the ICOM-CC 18th Triennial Conference, Copenhagen, Denmark, 4–8 September 2017; pp. 109–127.
32. Ward, C.; Giles, D.; Sully, D.; Lee, D.J. The conservation of a group of waterlogged neolithic bark bowls. *Stud. Conserv.* **1996**, *41*, 241–249.

33. Rao, H.; Yang, Y.; Hu, X.; Yu, J.; Jiang, H. Identification of an Ancient Birch Bark Quiver from a Tang Dynasty (A.D. 618–907) Tomb in Xinjiang, Northwest China. *Econ. Bot.* **2017**, *71*, 32–44. [[CrossRef](#)]
34. Tintner, J.; Smidt, E.; Aumüller, C.; Martin, P.; Ottner, F.; Wriessnig, K.; Reschreiter, H. Taphonomy of prehistoric bark in a salt environment at the archaeological site in Hallstatt, Upper Austria—An analytical approach based on FTIR spectroscopy. *Vib. Spectrosc.* **2018**, *97*. [[CrossRef](#)]
35. Kolattukudy, P.E. Suberin from Plants. In *Biopolymers*; Steinbüchel, A., Yosiharu, D., Eds.; Wiley: Weinheim, Germany, 2002; Volume 3a, pp. 41–73.
36. Agrawal, O.P.; Dhawan, S. Studies on fungal resistance of birch-bark. In Proceedings of the ICOM-CC 7th Triennial Meeting, Copenhagen, Denmark, 10–14 September 1984; pp. 1–3.
37. Ranathunge, K.; Schreiber, L.; Franke, R. Suberin research in the genomics era—New interest for an old polymer. *Plant Sci.* **2011**, *180*, 399–413. [[CrossRef](#)]
38. Parameswaran, N.; Wilhelm, G.E. Micromorphology of naturally degraded beech and spruce barks. *Eur. J. For. Pathol.* **1979**, *9*, 103–112. [[CrossRef](#)]
39. Rypacek, W. *Biologie Holzzerstörender Pilze*; VEB Gustav Fischer Verlag: Jena, Germany, 1966.
40. Zimmermann, W.; Seemüller, E. Degradation of Raspberry Suberin by *Fusarium solani* f. sp. *Pisi* and *Armillaria mellea*. *J. Phytopathol.* **1984**, *110*, 192–199. [[CrossRef](#)]
41. Ofong, A.U.; Pearce, R.B. Suberin degradation by *Rosellinia desmazieresii*. *Eur. J. For. Pathol.* **1994**, *24*, 316–322. [[CrossRef](#)]
42. Fernando, G.; Zimmermann, W.; Kolattukudy, P.E. Suberin-grown *Fusarium solani* f. sp. *pisi* generates a cutinase-like esterase which depolymerizes the aliphatic components of suberin. *Physiol. Plant Pathol.* **1984**, *24*, 143–155. [[CrossRef](#)]
43. Swift, J.M. Loss of Suberin from Bark tissue rotted by *Armillaria mellea*. *Nature* **1965**, *207*, 436–437. [[CrossRef](#)]
44. Kontkanen, H.; Westerholm-Parvinen, A.; Saloheimo, M.; Bailey, M.; Ratto, M.; Mattila, I.; Mohsina, M.; Kalkkinen, N.; Nakari-Setälä, T.; Buchert, J. Novel Coprinopsis cinerea polyesterase that hydrolyzes cutin and suberin. *Appl. Environ. Microbiol.* **2009**, *75*, 2148–2157. [[CrossRef](#)] [[PubMed](#)]
45. Ferreira, R.; Garcia, H.; Sousa, A.F.; Freire, C.S.R.; Silvestre, A.J.D.; Rebelo, L.P.N.; Pereira, C.S. Isolation of suberin from birch outer bark and cork using ionic liquids: A new source of macromonomers. *Ind. Crop. Prod.* **2013**, *44*, 520–527. [[CrossRef](#)]
46. Ferreira, R.; Garcia, H.; Sousa, A.F.; Petkovic, M.; Lamosa, P.; Freire, C.S.R.; Silvestre, A.J.D.; Rebelo, L.P.N.; Pereira, C.S. Suberin isolation from cork using ionic liquids: Characterisation of ensuing products. *New J. Chem.* **2012**, *36*, 2014–2024. [[CrossRef](#)]
47. Martins, I.; Hartmann, D.O.; Alves, P.C.; Martins, C.; Garcia, H.; Leclercq, C.C.; Ferreira, R.; He, J.; Renaut, J.; Becker, J.D.; et al. Elucidating how the saprophytic fungus *Aspergillus nidulans* uses the plant polyester suberin as carbon source. *BMC Genom.* **2014**, *15*, 613. [[CrossRef](#)]
48. Ursache, R.; De Jesus Vieira Teixeira, C.; Déneraud Tendon, V.; Gully, K.; De Bellis, D.; Schmid-Siegert, E.; Grube Andersen, T.; Shekhar, V.; Calderon, S.; Pradervand, S.; et al. GDSL-domain proteins have key roles in suberin polymerization and degradation. *Nat. Plants* **2021**. [[CrossRef](#)]
49. Tibbett, M.; Grantham, K.; Sanders, F.E.; Cairney, J.W.G. Induction of cold active acid phosphomonoesterase activity at low temperature in psychrotrophic ectomycorrhizal *Hebeloma* spp. *Mycol. Res.* **1998**, *102*, 1533–1539. [[CrossRef](#)]
50. Weinstein, R.N.; Montiel, P.O.; Johnstone, K. Influence of growth temperature on lipid and soluble carbohydrate synthesis by fungi isolated from fellfield soil in the maritime Antarctic. *Mycologia* **2000**, *92*, 222–229. [[CrossRef](#)]
51. Duarte, A.W.F.; dos Santos, J.A.; Vianna, M.V.; Vieira, J.M.F.; Mallagutti, V.H.; Inforsato, F.J.; Wentzel, L.C.P.; Lario, L.D.; Rodrigues, A.; Pagnocca, F.C.; et al. Cold-adapted enzymes produced by fungi from terrestrial and marine Antarctic environments. *Crit. Rev. Biotechnol.* **2018**, *38*, 600–619. [[CrossRef](#)]
52. Robinson, C.H. Cold adaptation in Arctic and Antarctic fungi. *New Phytol.* **2001**, *151*, 341–353. [[CrossRef](#)]
53. Björdal, C. Microbial degradation of waterlogged archaeological wood. *J. Cult. Herit.* **2012**, *13*, 118–122. [[CrossRef](#)]
54. Björdal, C.; Nilsson, T. Decomposition of waterlogged archaeological wood. In Proceedings of the 8th ICOM-CC WOAM Conference, Stockholm, Sweden, 11–15 June 2001; pp. 235–247.
55. Pedersen, N.B.; Björdal, C.G.; Jensen, P.; Felby, C. Bacterial Degradation of Archaeological Wood in Anoxic Waterlogged Environments. In *Stability of Complex Carbohydrate Structures: Biofuels, Foods, Vaccines and Shipwrecks*; Harding, S.E., Ed.; RSC Publishing: Cambridge, MA, USA, 2012; pp. 160–187.
56. Blanchette, R.A. A review of microbial deterioration found in archaeological wood from different environments. *Int. Biodeterior. Biodegrad.* **2000**, *46*, 189–204. [[CrossRef](#)]
57. Blanchette, R.A.; Nilsson, T.; Daniel, G.; Abad, A. Biological Degradation of Wood. In *Archaeological Wood*; Rowell, R.M., James Barbour, R., Eds.; Advances in Chemistry; American Chemical Society: Washington, DC, USA, 1990; Volume 225, pp. 141–174.
58. Blanchette, R.; Cease, K.; Abad, A.; Burnes, T.; Obst, J. Ultrastructural characterization of wood from Tertiary fossil forest in the Canadian Arctic. *Can. J. Bot.* **1991**, *69*, 560–568. [[CrossRef](#)]
59. Blanchette, R.A. Microbial degradation of wood from aquatic and terrestrial environments. In *Cultural Heritage Microbiology: Fundamental Studies in Conservation Science*; Mitchell, R., McNamara, C.J., Eds.; ASM Press: Washington, DC, USA, 2010; pp. 179–218.
60. Blanchette, R.A.; Held, B.W.; Jurgens, J.; Stear, A.; Dupont, C. Fungi attacking historic wood of Fort Conger and the Peary Huts in the High Arctic. *PLoS ONE* **2021**, *16*, e0246049. [[CrossRef](#)]

61. Matthiesen, H.; Jensen, J.B.; Gregory, D.; Hollesen, J.; Elberling, B. Degradation of Archaeological Wood Under Freezing and Thawing Conditions—Effects of Permafrost and Climate Change. *Archaeometry* **2014**, *56*, 479–495. [[CrossRef](#)]
62. Pedersen, N.B.; Matthiesen, H.; Blanchette, R.; Alfredeisen, G.; Held, B.; Westergaard-Nielsen, A.; Hollesen, J. Fungal attack on archaeological wooden artefacts in the Arctic-implications in a changing climate. *Sci. Rep.* **2020**, *10*, 8187. [[CrossRef](#)]
63. Hafner, A.; Klügl, J. Neolithisches Bogenfutteral aus Birkenrinde, Holz und Leder. In *Schnidejoch und Lötschenpass. Archäologische Forschungen in den Berner Alpen. Schnidejoch et Lötschenpass. Investigations Archéologiques dans les Alpes Bernoises*; Archäologischer Dienst Bern: Bern, Switzerland, 2015; Volume 2, pp. 15–18.
64. Junkmanns, J.; Klügl, J.; Schoch, W.H.; Di Pietro, G.; Hafner, A. Neolithic and Bronze Age archery equipment from alpine ice-patches: A review on components, construction techniques and functionality. *J. Neolit. Archaeol.* **2019**, *21*, 283–314. [[CrossRef](#)]
65. Klügl, J. How to conserve a birch bark bow case from an ice patch? In Proceedings of the 12th ICOM-CC Group on Wet Organic Archaeological Materials Conference, Istanbul, Turkey, 13–17 May 2013; pp. 270–278.
66. Pilø, L.; Finstad, E.; Barrett, J.H. Crossing the ice: An Iron Age to medieval mountain pass at Lendbreen, Norway. *Antiquity* **2020**, *94*, 437–454. [[CrossRef](#)]
67. Haeberli, W.; Alean, J. Temperature and accumulation of high altitude firn in the alps. *Ann. Glaciol.* **1985**, *6*, 161–163. [[CrossRef](#)]
68. Isaksen, K.; Holmlund, P.; Sollid, J.L.; Harris, C. Three deep Alpine-permafrost boreholes in Svalbard and Scandinavia. *Permafrost Periglac. Process.* **2001**, *12*, 13–25. [[CrossRef](#)]
69. Guthruf, K.; Maurer, V.; Ryser, R.; Zeh, M.; Zweifel, N. *Zustand der Kleinseen*; AWA Amt für Wasser und Abfall, Gewässer- und Bodenschutzlabor GBL: Bern, Switzerland, 2015.
70. Ghemawat, M.S. Polychromatic staining with toluidine blue O for studying the host-parasite relationships in wheat leaves of *Erysiphe graminis* f. sp. *tritici*. *Physiol. Plant Pathol.* **1977**, *11*, 251–253. [[CrossRef](#)]
71. Pedersen, N.B. *Microscopic and Spectroscopic Characterisation of Waterlogged Archaeological Softwood from Anoxic Environments*; University of Copenhagen: Frederiksberg, Denmark, 2015.
72. Sousa, A.F.; Gandini, A.; Caetano, A.; Maria, T.M.; Freire, C.S.; Neto, C.P.; Silvestre, A.J. Unravelling the distinct crystallinity and thermal properties of suberin compounds from *Quercus suber* and *Betula pendula* outer barks. *Int. J. Biol. Macromol.* **2016**, *93*, 686–694. [[CrossRef](#)] [[PubMed](#)]
73. Daniel, G.; Nilsson, T.; Pettersson, B. Poorly and Non-Lignified Regions in the Middle Lamella Cell Corners of Birch (*Betula Verrucosa*) and Other Wood Species. *IAWA J.* **1991**, *12*, 70–83. [[CrossRef](#)]
74. de Lhoneux, B.; Antoine, R.; Côté, W.A. Ultrastructural implications of gamma-irradiation of wood. *Wood Sci. Technol.* **1984**, *18*, 161–176. [[CrossRef](#)]
75. Parameswaran, N.; Wilhelm, G.E.; Liese, W. Ultrastructural aspects of beech bark degradation by fungi. *Eur. J. For. Pathol.* **1976**, *6*, 274–286. [[CrossRef](#)]
76. Singh, P.A. A review of microbial decay types found in wooden objects of cultural heritage recovered from buried and waterlogged environments. *J. Cult. Herit.* **2012**, *13S*, 16–20. [[CrossRef](#)]
77. Beaulieu, C.; Sidibé, A.; Jabloun, R.; Simao-Beauvoir, A.-M.; Lerat, S.; Monga, E.; Bernards, M.A. Physical, Chemical and Proteomic Evidence of Potato Suberin Degradation by the Plant Pathogenic Bacterium *Streptomyces scabiei*. *Microbes Environ.* **2016**, *31*, 427–434. [[CrossRef](#)] [[PubMed](#)]
78. Chowdhury, P.; Nag, S.; Ray, A. Degradation of Phenolic Compounds Through UV and Visible-Light-Driven Photocatalysis: Technical and Economic Aspects. *Phenolic Compd. Nat. Sources Importance Appl.* **2017**, *16*, 395–417.
79. Gandini, A.; Pascoal Neto, C.; Silvestre, A.J.D. Suberin: A promising renewable resource for novel macromolecular materials. *Prog. Polym. Sci.* **2006**, *31*, 878–892. [[CrossRef](#)]
80. Rosa, M.E.; Pereira, H.; Fortes, M.A. Effects of hot water treatment on the structure and properties of cork. *Wood Fiber Sci.* **1990**, *22*, 149–164.